

FABRICATION, SYNTHESIS, AND CHARACTERIZATION OF FLAME  
RETARDANT AND THERMALLY STABLE MATERIALS: FLAME RETARDANT  
COATING FOR POLYURETHANE FOAM AND FUSED-RING BENZO-/  
NAPHTHOXAZINES

by

JIACHENG LIU

Submitted for partial fulfillment of the requirements

For the degree of Master of Science

Thesis adviser: Dr. Hatsuo Ishida

Department of Macromolecular Science and Engineering

CASE WESTERN RESERVE UNIVERSITY

May, 2017

CASE WESTERN RESERVE UNIVERSITY

SCHOOL OF GRADUATE STUDIES

We hereby approve the thesis/dissertation of

Jiacheng Liu

candidate for the degree of Master of Science\*.

Committee Chair

Dr. Hatsuo Ishida

Committee Member

Dr. Rigoberto Advincula

Committee Member

Dr. Gary Wnek

Date of Defense

March 31<sup>st</sup>, 2017

\*We also certify that written approval has been obtained for any proprietary material  
contained therein.

## Table of Contents

Table of Contents .....	i
List of Tables .....	iii
List of Schemes .....	iii
List of Figures .....	iii
Acknowledgement .....	vi
Abstract .....	vii
Chapter 1. Very High Nanofiller-content Casein/laponite Nanocomposite Coating for Polyurethane Foam Flame Suppression through Single-dip Fabrication .....	1
1.1. Introduction .....	2
1.2. Experimental .....	6
1.2.1. Materials .....	6
1.2.2. Preparation of flame retardant polyurethane foam .....	6
1.2.3. Casein/ laponite nanocomposite fabrication.....	7
1.2.4. Characterization.....	7
1.3. Results and discussion.....	8
1.4. Conclusion.....	26
1.5. References .....	28
Chapter 2. Synthesis and Characterization of Fused-ring Benzo-/ naphthoxazines .....	33

2.1. Introduction .....	34
2.2. Experimental Section .....	36
2.2.1. Materials .....	36
2.2.2. Monomer synthesis.....	36
2.2.3. Characterization.....	40
2.3. Results and Discussion.....	41
2.4. Conclusions .....	53
2.5. References .....	54

## List of Tables

<b>Table 1.1.</b> Flame retardant and thermal stability data.....	22
<b>Table 2.1.</b> Characteristic vibration frequencies for oxazine ring for fused-ring benzo- /naphthoxazines.....	45
<b>Table 2.2.</b> Thermal stability values of polymerized fused-ring benzo-/naphthoxazines.	52

## List of Schemes

<b>Scheme 2.1.</b> Preparation of 1,3-benzoxazines through a) modified Mannich reaction of a phenol, primary amine and formaldehyde, and b) 3-step strategy.....	35
<b>Scheme 2.2.</b> Preparation of fused-ring benzo-/naphthoxazines. ....	42

## List of Figures

<b>Figure 1.1.</b> FT-IR spectrum of <b>a)</b> casein, <b>b)</b> laponite-50wt% nanocomposite, <b>c)</b> laponite- 30wt% nanocomposite, and <b>d)</b> laponite.....	10
<b>Figure 1.2.</b> X-ray diffractions of <b>a)</b> laponite, <b>b)</b> laponite-90wt% nanocomposite, <b>c)</b> laponite-50wt% nanocomposite, and <b>d)</b> laponite-30wt% nanocomposite.....	11
<b>Figure 1.3.</b> SEM images of fractured film surfaces: <b>a)</b> laponite, <b>b)</b> laponite-90wt%, <b>c)</b> laponite-50wt%, and <b>d)</b> casein.....	12
<b>Figure 1.4.</b> SEM image of morphology PUF and coated PUF surface: <b>a), b), c)</b> Pure PU foam, <b>d), e), f)</b> PUL50, and <b>g), h), i)</b> PUL90. ....	15
<b>Figure 1.5.</b> TGA spectrum of pure PU and coated PU foams.....	17

<b>Figure 1.6.</b> Digital photographs of residues after cone test: a) pure PU, b) PUL30, c) PUL40, d) PUL50, e) PUL60, f) PUL70, g) PUL80, and h) PUL90.....	20
<b>Figure 1.7.</b> HRR profile of PUF and coated PUFs.....	21
<b>Figure 1.8.</b> THR profile of PUF and coated PUFs.....	21
<b>Figure 1.9.</b> SPR profile of PUF and coated PUFs.....	23
<b>Figure 1.10.</b> TSP profile of PUF and coated PUFs.....	23
<b>Figure 1.11.</b> SEM image of residue char: a), b), c), d) residue of PUL50 and e), f), g), h) residue of PUL90. ....	24
<b>Figure 1.12.</b> HRR profiles of PUFs coated with casein(PUC) or laponite(PUL), and PUL90, pure PU.....	26
<b>Figure 2.1.</b> <sup>1</sup> H-NMR spectra of a) <b>1N-p-f</b> , b) <b>1N-p6-f</b> , c) <b>1N-dihq-f</b> , d) <b>35DMP-p-f</b> , e) <b>15DHN-p-f</b> , and f) PH-a.....	43
<b>Figure 2.2.</b> FT-IR spectra of a) <b>1N-p-f</b> , b) <b>1N-p6-f</b> , c) <b>1N-dihq-f</b> , d) <b>35DMP-p-f</b> , and e) <b>15DHN-p-f</b> .. ....	44
<b>Figure 2.3.</b> FT-IR spectra of a) <b>1N-p-f</b> , b) <b>1N-p6-f</b> , c) <b>1N-dihq-f</b> , and e) <b>15DHN-p-f</b> ..	46
<b>Figure 2.4.</b> DSC thermograms of a) <b>1N-p-f</b> , b) <b>1N-p6-f</b> , c) <b>1N-dihq-f</b> , d) <b>35DMP-p-f</b> , e) <b>15DHN-p-f</b> , and f) PH-a.....	47
<b>Figure 2.5.</b> FT-IR spectra of <b>1N-p-f</b> between the regions 4000-600 cm <sup>-1</sup> at a) rt, b) 120 °C for 1h, c) 130 °C for 30 min, d) 140 °C for 30 min, and e) 150 °C for 30 min.....	49
<b>Figure 2.6.</b> TGA thermograms of a) <b>poly(1N-p6-f)</b> , b) <b>poly(1N-p-f)</b> , c) <b>poly(1N-dihq-f)</b> , d) <b>poly(35DMP-p-f)</b> , and e) <b>poly(15DHN-p-f)</b> .....	51

**Figure 2.7.** Derivative of the weight loss as a function of the temperature of the fused-ring benzo-/naphthoxazines. .... 51

## **Acknowledgement**

My deepest appreciation goes to my parents who supported my life and study enthusiastically. Their warmest support is essential for me.

I would like to thank my adviser, Dr. Hatsuo Ishida for his patient advice and education. His guidance and encouragement are very fundamental to my academic pursuit. I would also like to thank my present and past group members, who helped me to improve.

Besides, I am grateful to Dr. Fumiaki Takahashi and SCSAM for their help in equipment.

Fabrication, Synthesis, and Characterization of Flame Retardant  
and Thermally Stable Materials: Flame Retardant Coating for Polyurethane  
Foam and Fused-ring Benzo-/naphthoxazines

**Abstract**

by

JIACHENG LIU

Reduction of fire hazard is essential to our sociality for saving human life and property. To achieve real-world attractive flame retardant materials, two approaches are seemingly feasible: imparting flame retardancy through simple and environmentally friendly method and developing intrinsically thermally stable materials. In this thesis, a flame retardant coating utilizing casein and laponite was investigated for polyurethane foam fire suppression. Quantitative techniques were utilized to study its efficiency and microscopic characterizations were conducted to propose flame retardant mechanism. Additionally, a series of novel thermosetting materials- namely fused-ring benzo-/naphthoxazines was synthesized and studies for their polymer form. Among these monomers, one particular case- **15DHN-p-f** showed attractive thermal stability as well as lower polymerization temperature.

# Chapter 1.

## Very High Nanofiller-content Casein/laponite Nanocomposite Coating for Polyurethane Foam Flame Suppression through Single-dip Fabrication

### **Abstract:**

Very high nanofiller content nanocomposite coating that consists of casein as a naturally abundant polymer matrix and non-exfoliated and/or non-intercalated laponite as an inorganic nanofiller reinforcement has been studied as an effective flame retardant for polyurethane foam (PUF). The ultra-thin coating is applied via single-dip method. Successful nanocomposite making is confirmed by Fourier transform infrared spectroscopy (FT-IR), X-ray diffraction (XRD), and scanning electron microscopy (SEM). Coated PUFs with high laponite concentration shows desirable flammability reduction. With 90 wt% laponite concentration, heat release rate (HRR) of the second peak, average heat release rate (aHRR), and total smoke production (TSP) are reduced by 57.0 %, 30.9 %, and 33.3%, respectively, as determined by cone calorimetric experiment. The barrier effect provided by casein/ laponite coating is discussed as the major flame retardant mechanism. This work demonstrates a simple, commercially applicable, and environmentally benign method for flame suppression.

## 1.1. Introduction

According to the report of National Fire Protection Association(NFPA), fire resulted 3280 civilian casualties among which home fire caused 2560 comprising 78% approximately in the United State of America during the year of 2015.<sup>1</sup> Polyurethane foam (PUF) as a soft material has been widely applied for upholstery comfort purpose in indoor furniture, mattress, and building industry. However, due to the high aliphatic content, large surface area, and good air permeability, PUF is extremely flammable characterized by susceptible to ignition, rapid fire spread, and large amount of heat release during combustion.<sup>2</sup> In addition to its flame hazard, toxic smokes and gases including CO and HCN released after ignition are even more lethally threatening to product users.<sup>3</sup> Conventional techniques commonly adopted to impart flame retardancy to PUF was incorporation of halogenated components. However, as halogenated flame retardant additives often rise potential toxicity to human body and environment, their application has recently been met with strict regulations in the U.S.A, and so does in other world major economies. Application of other types of flame retardant additives, such as phosphorous and nitrogen containing compounds, are often confronted by sacrificing physical properties.<sup>4-5</sup> Therefore, endowing flame retardancy to PUF with a nontoxic and environmentally friendly approach has attracted strong attention of researchers in recent years.

Recently, a novel treatment method which is termed layer-by-layer(LBL) deposition has firstly been systematically examined by Grunlan et al to demonstrate its effectiveness in flame retardancy improvement.<sup>6</sup> This technique applies polymers, such as chitosan,<sup>7</sup> poly(acrylic acid),<sup>8</sup> poly(ethylene imine),<sup>6</sup> ammonium polyphosphate,<sup>9</sup> alginate,<sup>10</sup> and

nanomaterials, montmorillonite(MMT),<sup>11</sup> vermiculite,<sup>12</sup> carbon nanofiber,<sup>13</sup> to fabricate flame retardant nanocoating on fabric or foam materials in an environmentally green manner. It is demonstrated by Kim et al that the carbon nanofiber filled multilayer (with 4 bilayers) coating could reduce the PHHR of PUF by 40% and simultaneously eliminate the melt dripping.<sup>13</sup> The same group later examined that naturally occurring clay-montmorillonite is also capable of being a multilayer coating component to suppress PUF's flammability,<sup>14</sup> And MMT content in the layer-by-layer coating plays a critical role in improving flame retardant properties, saying higher MMT concentration resulting more dramatic reduction on flammability.<sup>15</sup> Cain et al studied that high aspect ratio of clay can lead to better flammability performance, that 4 bilayers of polymer/MMT coating is needed to suppress single bilayer of polymer/vermiculite coating in terms of HRR.<sup>12</sup> Besides inorganic fillers used in LBL coating, lignosulphonate partnered with chitosan is able to reduce the PHRR of PUF by 43% with 8 bilayers.<sup>16</sup> Due to its promising flame retardancy performance in addition to environmentally friendly processing, LBL technique has been continuously drawing scientific and industrial attention. However, as the underlying procedure of this fabrication technique requires consecutive dipping process of the substrate into solution or suspension of the coating component and subsequent washing for each layer placement, large scale application requires significant simplification of the process.

In an effort to create flame retardant coating aligned with the “green” methodology with LBL technique, few other works have been carried out featuring less complicated processing. Davis et al successfully demonstrated that a bioinspired one-pot coating (starch and sodium polyborate) can reduce PUF's PHHR by 75% with a coating uptake of 155%.<sup>17</sup>

An alginate/clay aerogel coating has been employed to impart flame retardancy to PUF, which reduced PHRR from 323 KW/m<sup>2</sup> of neat PUF to 20 KW/m<sup>2</sup>, but simultaneously increased 2.24 times of specific modulus.<sup>18</sup> Sol-gel deposition method applying organosilane and diethyl phosphate also proved to provide PHRR reduction by 60% and self-extinguishing property according to the UL-94 standard to PUF.<sup>19</sup> These pioneering researches are able to improve flammability of PUF to a satisfying level. But it would be more attractive to achieve a flame retardant coating through simple processing technique without significantly influencing PUF's physical property.

Casein is a naturally abundant polymer consisting approximately of 80% of protein of bovine milk. It is a family of phosphoproteins ( $\alpha$ 1-casein,  $\alpha$ 2-casein,  $\beta$ -casein, and  $\kappa$ -casein) with molecular weight of 19-25 kDa and isoelectric point of 4.2-5.8.<sup>20</sup> Each of these phosphoproteins has its unique amino acid composition, with  $\alpha$ 1-casein containing 8-10 phosphate groups and  $\beta$ -casein contains 4-5 phosphate groups as two major phosphorous resources. Due to its high degree of molecular chain flexibility and large portion of nonpolar groups, casein presents excellent film-making, coating, and gas barrier properties. As a result, it has been investigated as adhesives,<sup>21</sup> and food packagings,<sup>22</sup> in addition to its primary application in food industry. In a recent study, casein has been examined as flame retardant coating that is able to reduce PHRR of cotton fabric by 27% with approximately 20% uptake.<sup>23</sup> The flame retardation mechanism was proposed to be a favored char forming over cellulose thermo-decomposition due to phosphoric content of casein. By the reasons of water solubility, bio-renewability, and phosphorous containing, casein is a favorable candidate for flame retardant coating fabrication through an environmentally friendly way.

Formulation of nanocomposite coating has been shown to improve flammability characteristics to PUF due to the block of diffusion effect of nanoparticles.<sup>24</sup> Laponite as a synthetic clay is consists of stacked layers of coin-like single which composed of one layer of edge-shared octahedra of  $\text{Al}^{3+}$  or  $\text{Mg}^{2+}$ , sandwiched between two layers of corner-shared tetrahedra of  $\text{Si}^{4+}$ .<sup>25</sup> It undergoes face-to-face packing of each individual platelet as aggregated state, but swells or exfoliates in water dispersion affording negative charge on the faces. At the edge of individual platelet, the oxygen atoms and hydroxyl groups are able to accept or release protons depending on the environment property. This nanomaterial presents a coin-like shape with approximately 25nm in diameter and 1nm in thickness of individual layers.

In this present work, a one-pot dipping approach to create casein/ laponite nanocomposite coating was studied for its effectiveness in suppressing flammability of PUF. Of particular interest is the preparation and its property of very high nanofiller-content nanocomposite coating far beyond the concentration of the majority of nanocomposites reported in the literature. Since both laponite surface and dissolved casein are both negatively charged, intercalation or exfoliation of the silicate layer is not intended: however, good processability and each of coating application are to be the advantages of the current approach. While the intended material is somewhat different from traditionally reported silicate-based nanocomposites where intercalation and exfoliation are intended, the current system studied can also be regarded nanocomposite due to the small size, 25 nm, of laponite used, despite the appearance of usual clay filled polymer. In this respect, the system studied is synonymous to silica nanofiller added polymer, except that the filler shape is platelet made up of aggregated single layer. This study focuses on examining

relationship between inorganic filler concentration and flammability through cone calorimetry. Thermal stability of coated PUF was also investigated by TGA. Flame retardant mechanism of casein/ laponite coating was discussed with results gained from TGA and SEM of char residue. This study might provide constructive visions to flame retardant coating fabrication of PUF using a sustainable green approach.

## **1.2. Experimental**

### **1.2.1. Materials**

Casein (technical grade, Mw=19k-25k) from bovine milk was purchased from Sigma-Aldrich. Sodium laponite (Laponite® grade B) was received from Southern Clay Company. Sodium Hydroxide (NaOH) (97%) was purchased from Fisher Chemical. Commercially available polyurethane foam (high density) was supplied by Mybecca, Inc. (CA, U.S.A.). 18MΩ deionized (DI) water was used to prepare all the solutions and suspensions. Casein was dissolved in 0.17 M NaOH aqueous solution at concentration of 10wt% and then diluted to 2wt% with DI water before formulation. Laponite was dispersed in DI water at concentration of 2wt% through ultrasonication with Brandson Ultrasound at 50% amplitude for 4 hrs. Polyurethane foam was sampled with dimensions of 10cm×10cm×2.5cm before coating fabrication and cone calorimetry testing.

### **1.2.2. Preparation of flame retardant polyurethane foam**

Casein/laponite coatings with laponite content of 30wt%, 40wt%, 50wt%, 60wt%, 70wt%, 80wt%, and 90wt% were prepared using as following procedure. Desired amount of 2wt% casein solutions was added to 2wt% laponite suspensions with various weight ratio under constant stirring to achieve casein/ laponite blend with 2wt% total solid

concentration. After mixing, the casein/laponite aqueous blends were stirred for 24 hrs for further homogenization. Polyurethane foam was immersed into above yielded casein/laponite aqueous mixture in very short time and then excess amount of mixture was squeezed out with a constant force. Water, as a solvent for coating process, was evaporated by drying the foam at 45°C in an oven. Control foam was made with the same procedure except for being immersed in to water instead of casein/laponite aqueous blend. Casein/laponite coated foams, with laponite coating content of 30wt%, 40wt%, 50wt%, 60wt%, 70wt%, 80wt%, and 90wt%, and control foam were named as PUL30, PUL40, PUL50, PUL60, PUL70, PUL80, PUL90, and PU, respectively. Same procedure was applied to obtain casein(PUC) and laponite(PUL) coated foams.

### **1.2.3. Casein/ laponite nanocomposite fabrication**

Casein solution and laponite suspension at various weight ratio were mixed aqueously under vigorous stirring for 24h. Then the resulted casein/ laponite colloidal suspensions were casted on petri dish to allow water evaporation at 45°C. As above method prepared film (laponite 50wt%, laponite 70wt%, and laponite 90wt%) was semi-transparent and brittle.

### **1.2.4. Characterization**

FT-IR utilizing Bomem Michaelson MB 110 spectrophotometer which is equipped with a deuterated triglycine sulfate detector was used to record FT-IR spectra of the samples. 32 scans were co-added per spectrum at a resolution of 4 cm<sup>-1</sup> after purging the spectrometer with dry air. Powder and solid samples were ground with KBr powder and pressed to form a 13 mm pellet for IR spectra recording in the absorbance mode.

Thermogravimetric analysis (TGA) was conducted on a TA instruments 2950 TGA with a heating rate of 10 °C/min under nitrogen at a flow rate of 60 mL/min. Combustion behavior was measured with cone calorimeter (Fire Testing Technology, UK) according to ASTM E 1354 standard procedures. PU specimens with dimensions of 10cm×10cm×2.5cm were subjected to the test under 35 KW/m<sup>2</sup> external heat irradiation with 24 L/s exhaust flow rate. All samples were placed in aluminum foil pan with only top surface exposed to applied heat. SEM was conducted with a Nova Nanolab 200 FEG-SEM/FIB for high resolution electron scanning microscopy. SEM samples were sputter-coated with a thin layer of gold before testing. X-ray diffraction was characterized on reflection mode with a Bruker Discover D8 X-ray diffractometer which was equipped with a monochromated X-ray source (Co K $\alpha$ ) and a 2D VÅNTEC-500 solid state detector.

### 1.3. Results and discussion

#### Casein/ laponite nanocomposite

To characterize the casein/ laponite nanocomposite, model films without the PU substrate were casted by employing the water evaporation procedure which is identical to the flame retardant coating fabrication. **Figure 1.1** shows the FT-IR spectra of the model casein/ laponite at the laponite concentration of 50wt%, 70wt%, and 90wt% system along with the raw material, casein and laponite. The bands that are commonly associated with casein are located at 1639 (Amide I band), 1519 (Amide II band), 1442 (C-H deformation), and 1229 cm<sup>-1</sup> (N-H deformation).<sup>26</sup> The characteristic laponite bands were observed at 1070 cm<sup>-1</sup> and 703 cm<sup>-1</sup>, which corresponds to Si-O stretching and O-Si-O bending, respectively.<sup>27</sup> Spectrum of nanocomposite (laponite 50wt%, laponite 70wt%,

and laponite 90wt%) showed that the peak at  $1519\text{ cm}^{-1}$  shifted to higher wavenumber of  $1537\text{ cm}^{-1}$ , which could be attributed to the hydrogen bonding formation between hydroxyl group of laponite and amine groups of casein. There are two potential sites of hydrogen bonding formation between the surface hydroxyl groups and amide group, namely  $\text{OH}\dots\text{HN}$  and  $\text{OH}\dots\text{O}=\text{C}$  bonds. However, when hydrogen bonding is formed with the carbonyl group, it is predicted to reduce its frequency whereas interaction with the secondary amine group increases the Amide band II frequency.<sup>28</sup> Thus, formation of hydrogen bonding between the surface hydroxyl groups of laponite and secondary amine group of casein is hypothesized. Furthermore, FTIR analysis indicates that there is no covalent bonding forming between the casein and laponite. The data supports our conclusion due to the lack of differences among the wavenumbers in the covalent range of the FTIR data (over  $1000$  up until  $2800\text{ cm}^{-1}$ ).

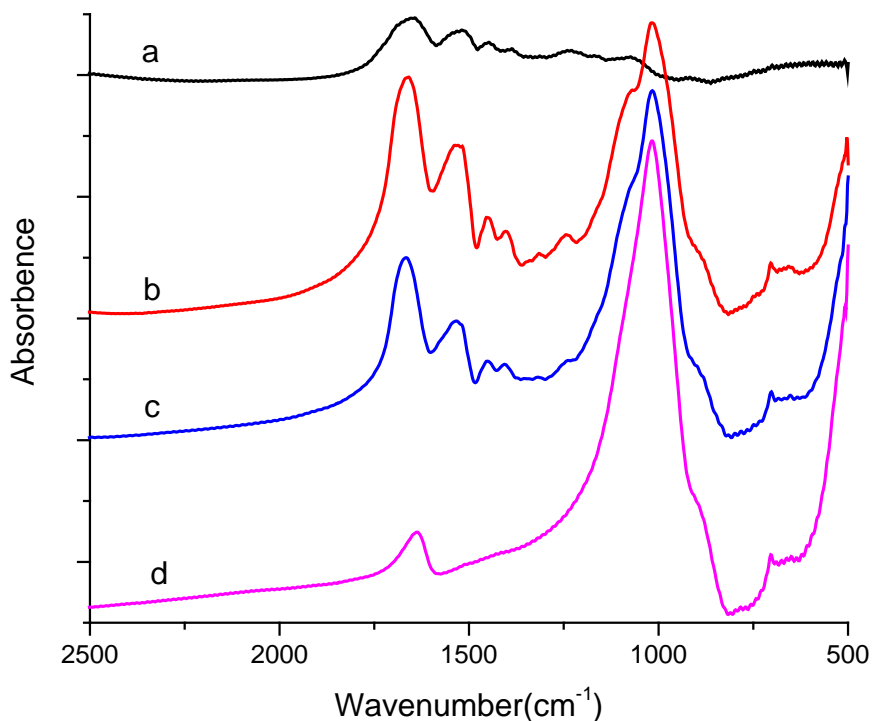


**Figure 1.1.** FT-IR spectrum of **a)** casein, **b)** laponite-50wt% nanocomposite, **c)** laponite-30wt% nanocomposite, and **d)** laponite.

In order to study whether laponite was intercalated with casein, X-ray diffraction in reflection mode was adopted to characterize the d-spacing between laponite single layer (**Figure 1.2**). Laponite powder sample showed  $2\theta$  peak at 8.99 degree, corresponding to d-spacing of 1.14 nm agreeing to the theoretical value.<sup>29</sup> XRD spectrum of laponite 50wt%, laponite 70wt%, and laponite 90wt% nanocomposites presented  $2\theta$  peaks at 8.57, 8.34, and 7.73 degrees, corresponding to d-spacing of 1.19 nm, 1.23 nm, and 1.33 nm, respectively. The increment of the d-spacing is less than the diameter of a hydrocarbon chain. Thus, the difference of d-spacing of interlayer between laponite powder and nanocomposite did not suggest an intercalated laponite. This result is understandable because of the repulsive

nature of the same negative electrical charge of both casein and laponite basal groups. As the casein concentration increases, the electrostatic interaction between laponite edge negative charge groups and casein positive charge groups becomes prominent so that increase laponite interlayer spacing. But electrical repulsion prevents casein further penetrate in to laponite interlayers. In summary, through the aqueous fabrication process, high laponite filler content nanocomposite was obtained, in which laponite as small aggregated nanoparticles dispersed homogeneously without intercalation or exfoliation.

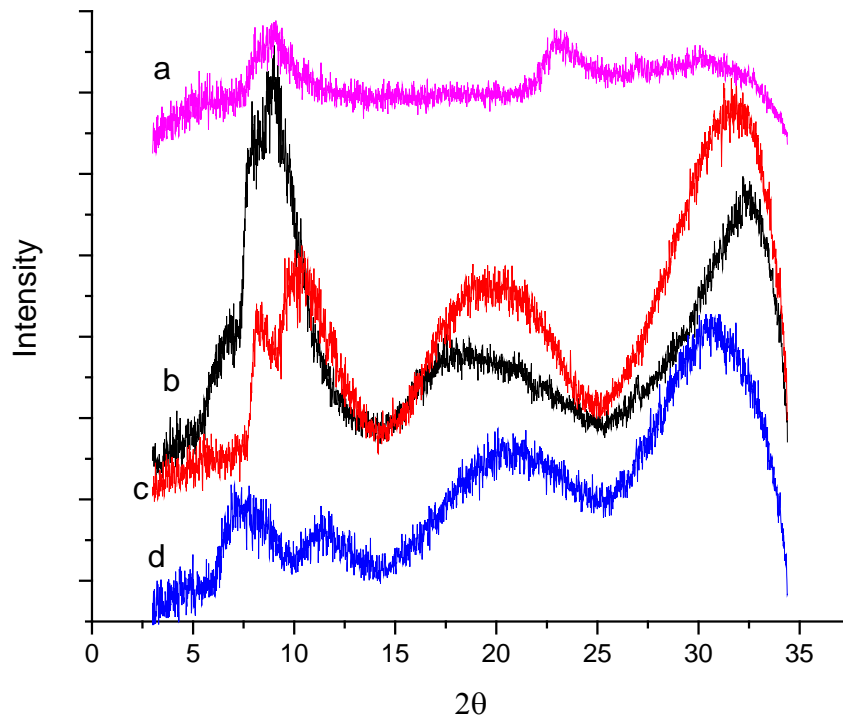


**Figure 1.2.** X-ray diffractions of **a)** laponite, **b)** laponite-90wt% nanocomposite, **c)** laponite-50wt% nanocomposite, and **d)** laponite-30wt% nanocomposite.

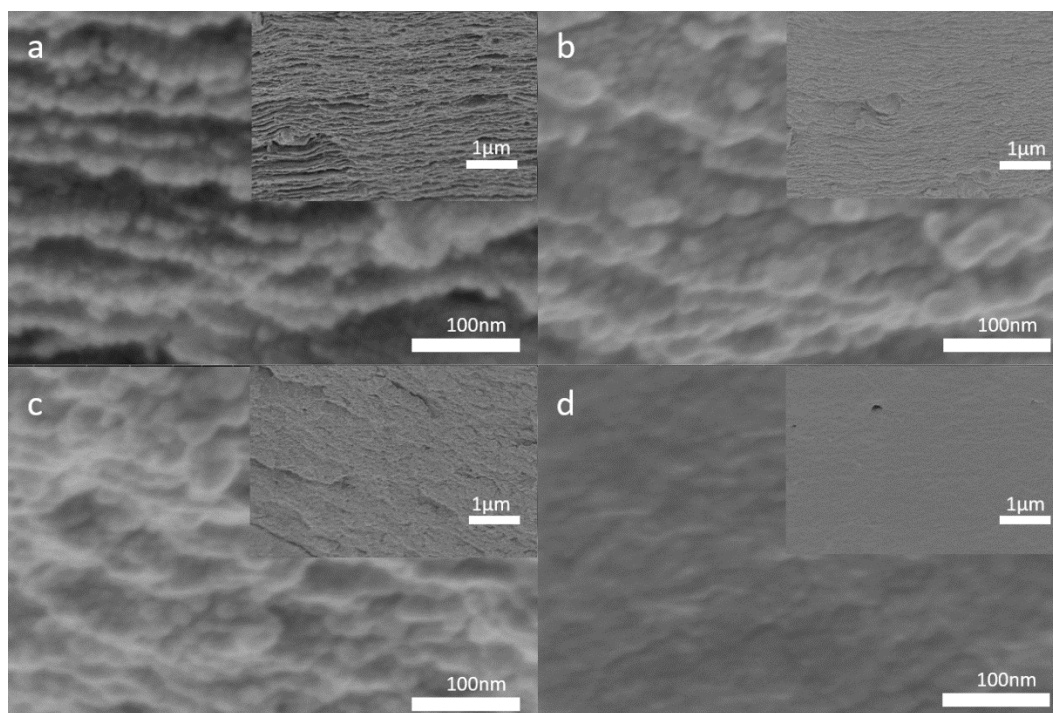


**Figure 1.3.** SEM images of fractured film surfaces: a) laponite, b) laponite-90wt%, c) laponite-50wt%, and d) casein.

SEM imaging was utilized to characterize the cross-sectional morphology of fractured laponite, laponite-50wt%, laponite-90wt%, and casein films. As it is shown in Figure 3, the overall cross-section of laponite film is extremely textured with sheet-like pattern. Meanwhile, casein film shows a rather smooth cross-section. At laponite concentration of 50wt%, sheet-like pattern could be hardly recognized. With 90wt% laponite, the sheet-like pattern becomes visible but still presents a reduced surface roughness. The overall behavior of reduced roughness suggests that the presence of casein acts as binder to laponite which will result in an improved mechanical property. In the laponite filled samples, nano-sized beads can be found with similar size as the original laponite used (approximately 25 nm in diameter). This situation is different from the morphology of nanoparticles in many nanocomposite papers reported. For the majority of

nanocomposite papers, the orientation of the basal plane of the nanofillers, such as silicate layers, are random whether they be intercalated or exfoliated. Such random orientation is not efficient for blocking the diffusion of fragmented, polymer free radical chains, while the efficiency of exfoliated layers would be better than the aggregated. In the current paper, the orientation of the laponite fillers appear to be in the x-y plane and little evidence is observed for the z-direction orientation, allowing the nanofillers to tightly packed. Also, the interparticle distance in the z-direction is extremely small. The molecular weight of the casein used is around 20 kDa and thus the radius of gyration is on the order of a few nm. Therefore, the casein molecules on the order of several nm thickness are expected to be all nanoconfined by the laponite surfaces since the distance of nanoconfined polymer is reported to be about two radii of gyration of the polymer used. It is not known, however, if such nanoconfined layer acts as deterrent for the diffusion of free radical polymer chain fragments or acceleration. On one hand, the mobility of the nanoconfined chains are restricted, resulting in a loss of glass transition phenomenon. On the other hand, the density of the polymer near the nanoparticle surface is reported to be rarefied allowing more free volume to be present, thus space for diffusion to be greater. Further detailed study is needed to evaluate the effect of the nanoconined matrix. However, it is safe to conclude that well aligned laponite particles in the x-y direction will effectively block the diffusion of the free radical fragments by the effective tortuous path effect, thus reducing the flammability of those radicals. As an identical method was employed in both flame retardant coating and model film fabrication, it is reasonable to assume that above characteristics are ~~is~~ representative of the casein/ laponite nanocomposite coating. In this work, the laponite was dispersed in the casein matrix as nanoscale aggregations, rather than

exfoliated or intercalated particles. This might suggest that after the aqueous mixing process, casein/ laponite colloids went through a self-packing process to form the high inorganic filler content nanocomposite coating.

### **Casein/ laponite nanocomposite coating fabrication on PU foam**

Surface engineering techniques have been widely studied to impart flame retardancy to various materials. The recently developed layer-by-layer deposition method is of great interest for scientist due to the green fabrication process and satisfying flame retardancy improvement for large surface area materials such as PU foams and fabrics without strongly impacting the bulk material properties and aesthetics.<sup>13</sup> However, this emerging technique typically requires many steps of alternating dipping to a treating solution and subsequent to allow for a sufficient amount of coating to be adsorbed. A recent work trying to reduce the fabrication process by in-situ forming aerogel on PU foam was reported.<sup>18</sup> The flame retardacy improvement was dramatic but a freeze-drying process was introduced which is not uncomplicated for scale up. To achieve our nanocomposite coating on PU foam surface in the current paper, a single-step dip-coating process was adopted. The PU foam was firstly immersed into the casein/ laponite suspension. Then excess amount of the coating suspension was pressed out, so that a very small amount was allowed to maintain on PU foam surface. After being dried at room temperature, coating content of PU specimens were determined to be nearly constant at 4.9%, 4.7%, 5.2%, 5.3%, 4.7%, 5.0%, and 4.9% for PUL30, PUL40, PUL50, PUL60, PUL70, PUL80, and PUL90, respectively. SEM was employed to study the surface morphology difference between untreated PU and treated PU foams. As it is shown in **Figure 1.4**, the pure PU foam presents a clean and smooth surface without roughness. After coating deposition process, PU with a 50wt%

laponite-coating shows a mostly smooth appearance but contains localized cracks and rugs. As the inorganic filler content increased to a very high amount (90wt% laponite), PU developed cracked textures spreads on the surface, which might be due to the poor mechanical property of very high filler content nanocomposite coating. The overall open-cell morphology of PU foam was not affected by addition of nanocomposite coating as the thickness of the coating used was extremely thin. For both PU and PU with coating, no significant aggregation could be found on the PU surface, suggesting that the simple dip-coating deposition process is capable of affording a homogeneous coating. The water evaporation initiates the self-packing process of casein/ laponite colloid.

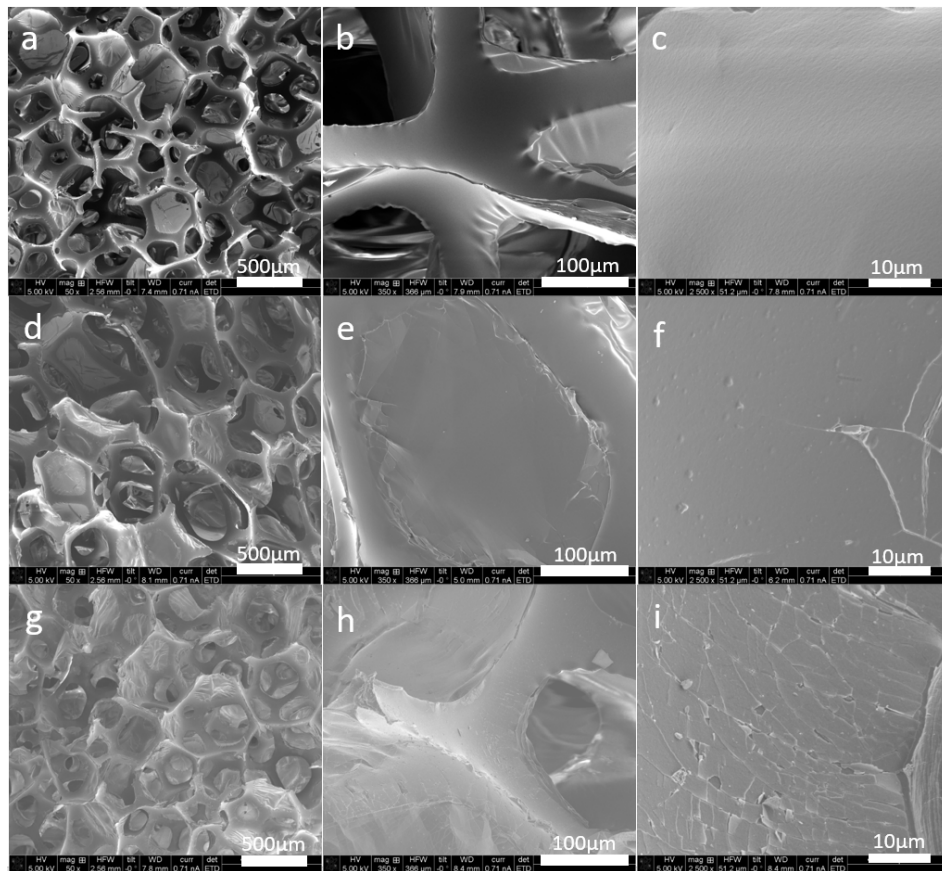


**Figure 1.4.** SEM image of morphology PUF and coated PUF surface: a), b), c) Pure PU foam, d), e), f) PUL50, and g), h), i) PUL90.

## Thermal stability

TGA was used to characterize the thermal degradation of PU foam and treated flame retardant PU foam under nitrogen atmosphere. The nitrogen atmosphere pyrolysis allows to simulate the degradation mechanism in condensed phase which is also under an oxygen-deficient condition. As the TGA curves showed in **Figure 1.5**, the pure PU foam undergoes two main thermal degradation steps. The first degradation step initiated at 190°C and finished at 390°C, which is believed to be responsible for urethane and urea bond breakage, generating polyols and isocyanate. At higher temperature range, regenerated polyol is responsible for the secondary step.<sup>30</sup> Its char yield was 1.01% at 700°C, indicating that there was negligible char formation and nearly all the PU foam was decomposed and evaporated. However, PUL30 showed a small increase of char yield to 1.93% and as laponite concentration increased to 90wt%, PUL90 presented the highest char yield of 7.32%. The inorganic laponite content is responsible for the char yield increased. Onset temperature of the degradation of the coated samples did not show significant variation and they preserve two-steps degradation profile, suggesting that casein/ laponite coating did not chemically changed the path way. A trend of delaying weight loss at higher temperature range can be observed as laponite concentration increases. This might indicate that casein/ laponite coating synergized the char forming stage and helped produce a more stable char which slows the decomposition. This might be achieved by the high nanofiller nanocomposite altering the rheological and other physical properties of the liquefied material who represents the mesophase where significant decomposition and diffusion of the materials take place. Overall character of TGA profiles suggest that casein/ laponite

coating could make PUF's thermal degradation less severe and laponite concentration played more important role in this process.

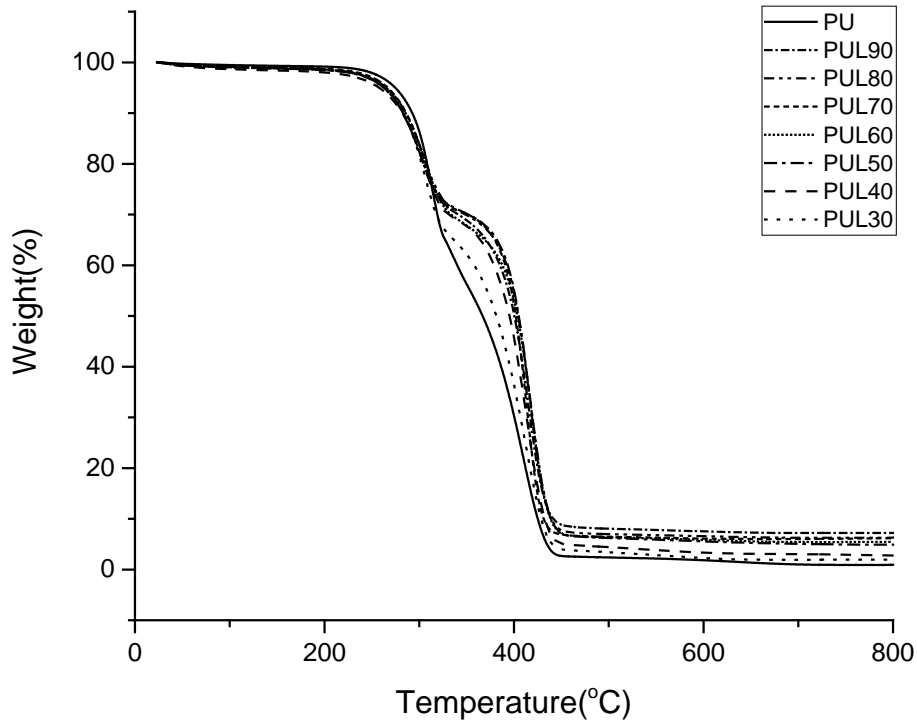


**Figure 1.5.** TGA thermograms of pure PU and coated PU foams.

### Flammability

Cone calorimeter is a technique widely utilized for evaluation of flammability in terms of heat release as well as smoke production upon combustion. Flammability parameters gained from the experiment, such as heat release rate (HRR), total heat release (THR), time to ignition(TTI), smoke production rate(SPR), and total smoke production(TSP), are key to assess the threat of a material when it is in exposure to real fire. HRR and THR data are presented in **Figures 1.6** and **1.7**, respectively, and related

values are summarized in **Table 1.1**. A typical heat release profile of polyurethane foam consists of two significant peaks, which represent the pyrolysis of isocyanate (first peak) and the later of polyol (second peak).<sup>31</sup> The untreated polyurethane foam in this work behaved consistently, showing two heat release peaks which are 321 KW/m<sup>2</sup> and 346 KW/m<sup>2</sup> respectively, releasing 18.3 MJ/m<sup>2</sup> as total heat release (THR). The second heat release peak is responsible to peak heat release rate (PHRR), occurring after 42 s of ignition. Ignition took place in 3 s (TTI) after the specimen being exposed to external heat and simultaneously applied ignition spark. Flammability of PU foams coated with the flame retardant coating with increasing laponite concentration was studied to examine the role of the two components. While the coating content of studied PU foams were not exactly identical, the variation is in a tolerant range for the purpose of unveiling a trend with 7 increments of samples. Ignition time (TTI) of all PU foam samples are 2-4 s, rendering no significant trend to be found. Two HRR peaks were found for all the samples which is the same as pure PU foam. The first HRR peak of PUL30 (who has the lowest laponite coating-concentration: 30 wt%) was 381 KW/m<sup>2</sup>. It gradually decreased to 295 KW/m<sup>2</sup> with PUL90 as the laponite concentration in the coating increased to 90wt%. Time to first peak also reduced from 21 s of pure foam to 6 s of PUL90. It is possible that this reduction of the time to first peak is due to the burning of the flammable, aliphatic portion of casein, rather than PU. Significant reduction of the second peak was found for the coated PU foams. All the coated samples showed reduction of second HRR peak compared to the pure PU foam. The second HRR peak of PUL30(344 KW/m<sup>2</sup>) and PUL40(300 KW/m<sup>2</sup>) showed slight reduction. However, a tendency of increasing peak reduction was found concurrent with increasing laponite concentration. The second peak of PUL90 disappeared and

became a plateau at level of 148 KW/m<sup>2</sup>, presenting a reduction as high as 57.0 % compared to the second peak of pure PU foam. The drastic reduction of HRR indicates the coated flame retardant PU foam presents a lower capacity of spreading flame to other materials and the potential of flame self-propagating under external heat radiation. In addition to HRR reduction, average heat release rate (aHRR) also showed a reduction of 30.9% of PUL90, decreased from 130 KW/m<sup>2</sup> of pure PU foam to 90 KW/m<sup>2</sup>. Overall HRR profiles of coated PU foams are characterized by: a quick reach of first peak which could be attributed to the earlier activation of casein/ laponite coating, followed by HRR drop down due to the protective char layer formation during combustion, and second peak or plateau arises resulting from the protective char breaking and polyol pyrolysis. Deeper drop down after first peak and broader plateau of HRR suggest a more effective protective layer formed due to the casein/ laponite coating. The best flame retardant performance (in terms of HRR, THR, aHRR, and char residue) was found of PUL90 which possesses the highest laponite coating-concentration (90wt%). As it is shown in **Figure 1.6** (photographs of residues after cone test), pure PU has totally burned out with no residues left. However, coated PU foams all showed char formation to some extent. Even the PUL30 which did not have obvious flame retardancy improvement presented residue formation. With laponite coating-concentration increases, residue structure gradually develops to the best with PUL90, becoming almost the same size and shape of original foam before burning. THR is an evaluation of total heat release during the combustion process, which is determined by the chemical decomposition of material. **Figure 1.8** shows the THR profiles of coated PU foams and control and THR values are summarized in **Table 1.1** Compared with control foam, coated samples did not present significant reduction of THR while the

curves became less steep. This might suggest that the casein/ laponite coating did not change chemical decomposition path way of PU foam and, meanwhile, the flame retardant mechanism could be mainly attributed to the shielding effect by the inorganic char.

As the residues formed after cone experiment maintained the foam-like structure (**Figure 1.6**), it is self-evident that the melting of PU by the flame was eliminated by casein/ laponite coating. This is further supporting observation of the modification of the rheological properties of the mesophase. Uncoated foam undergoes fast flame development due to the melting behavior. The melt pool releases a high amount of heat and promotes fire spreading. Coated PU foams form protective char, which helps to prevent melting or dripping during combustion, resulting in a slower HRR. An absence of melting or dripping is advantageous when considering to delay the fire spreading rate. In addition to improvement of reduction of HRR, this enhancement of anti-flammability also makes the casein/ laponite flame retardant coating even more attractive.



**Figure 1.6.** Digital photographs of residues after cone test: a) pure PU, b) PUL30, c) PUL40, d) PUL50, e) PUL60, f) PUL70, g) PUL80, and h) PUL90.

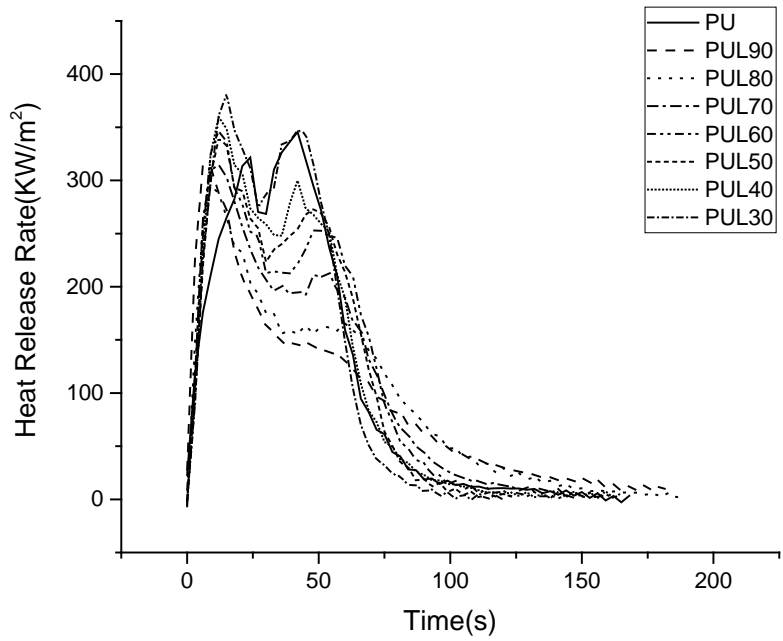


**Figure 1.7.** HRR profile of PUF and coated PUFs.

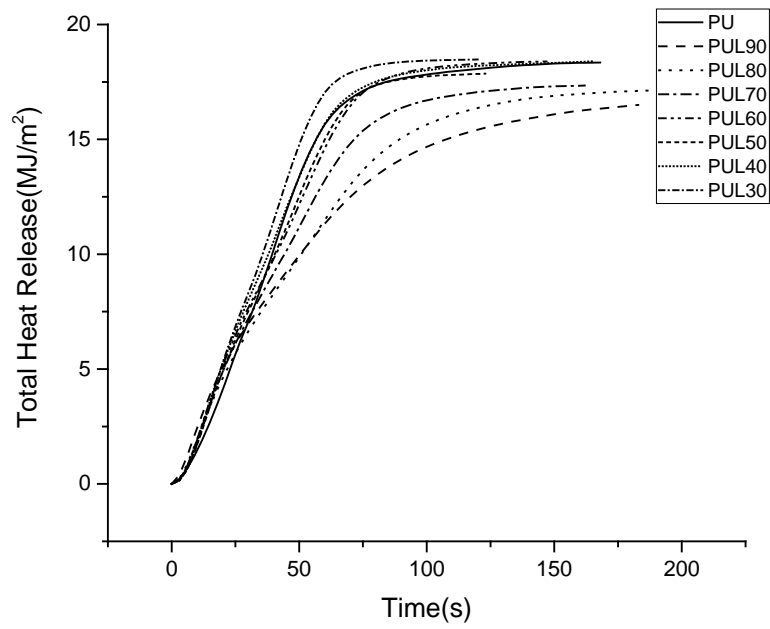


**Figure 1.8.** THR profile of PUF and coated PUFs.

**Table 1.1.** Flame retardant and thermal stability data.

	Coating mass %	Laponite concentration (wt%)	TTI (s)	First HRR Peak (KW/m <sup>2</sup> )	Second HRR Peak (KW/m <sup>2</sup> )	THR (MJ/m <sup>2</sup> )	TSP (m <sup>2</sup> /m <sup>2</sup> )	Char residue % At 700°C
PU			3	321	346	18.3	1.32	1.01
PUL30	4.9	30	3	381	344	18.4	1.35	1.93
PUL40	4.7	40	2	360	300	18.3	1.43	3.02
PUL50	5.2	50	3	339	273	17.8	1.42	5.06
PUL60	5.3	60	4	346	253	18.3	1.56	5.43
PUL70	4.7	70	4	315	211	17.3	1.43	6.03
PUL80	5.0	80	3	295	165	17.1	1.11	6.26
PUL90	4.9	90	3	315	148	16.4	0.88	7.21

### Smoke production

With respect to real fire hazard, smoke produced during fire often cause more human fatality, because of the toxicity of smoke particles and CO and blockage of the escape pathways. Therefore, reduction of smoke production is as important as HRR reduction in evaluating flammability. As TSP profile shown in **Figure 1.10**, TSP of neat PUF in this study was 1.32 m<sup>2</sup>/m<sup>2</sup>. Coated samples of PUL30, PUL40, PUL50, PUL60 and PUL70 did not have TSP reduction but show increase instead, whereas the smoke production time period spread wider and homogeneously than untreated PU form. However, when laponite concentration exceeded 70wt%, PUL80 and PUL90 both presented TSP of 1.11 m<sup>2</sup>/m<sup>2</sup> and 0.88 m<sup>2</sup>/m<sup>2</sup>, with reduction of 15.9% and 33.3%, respectively. The barrier effect of laponite is responsible for the TSP reduction, as it does not allow smoke to escape. High casein concentration activates ignition and dilute the barrier effect that leads to an increased TSP.

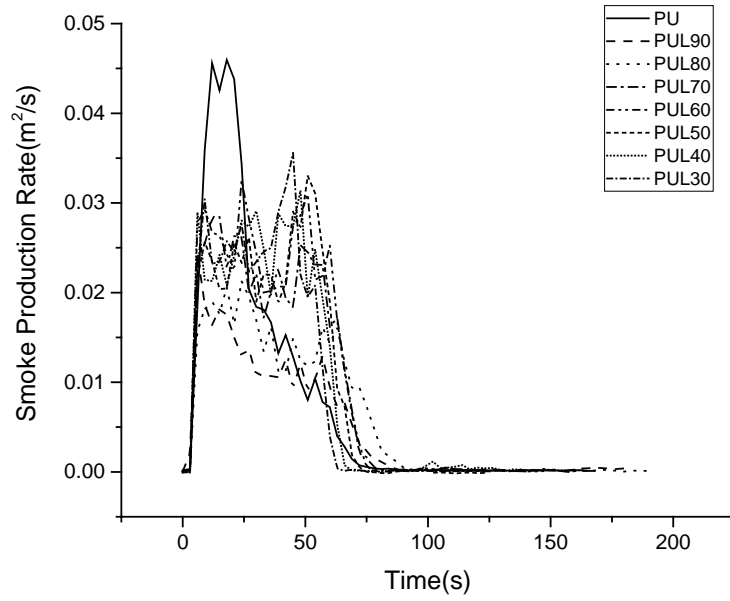


**Figure 1.9.** SPR profile of PUF and coated PUFs.

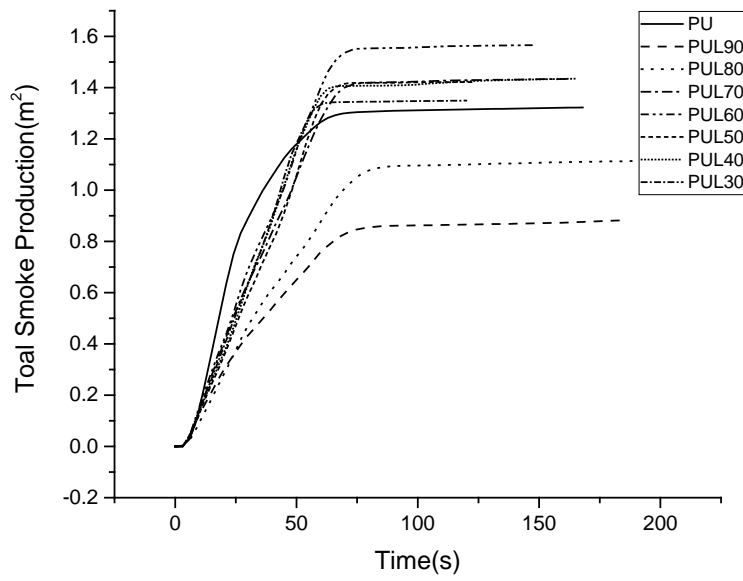


**Figure 1.10.** TSP profile of PUF and coated PUFs.

## Structure of combustion residue

The char residue after cone calorimetry experiment of PU and coated PU was characterized by SEM (**Figure 1.11**). The structure of residue from both PU and coated PU were disordered comparing with original foam. But the overall foam-like structure was maintained and only limited breakage and collapse was found, indicating a mechanical integrity of the char. The char formed after combustion was compact and showing a surface with homogeneously distributed small bubbles. These small bubbles might be formed during the intumescent process of casein combustion, as casein contains a certain amount of phosphorous element.<sup>23</sup> However, compared with the overall range of char region, the size and amount of bubble was not large and sufficient enough to cover a significant portion of the surface. As intumescence requires a prominent effect of carbonaceous bubbling which could trap air to prevent massive heat and small molecules (oxygen and combustibles) transfer,<sup>32</sup> the insufficient bubbling effect in this work suggests that the dominant flame retardant mechanism was the shielding effect of char formed.

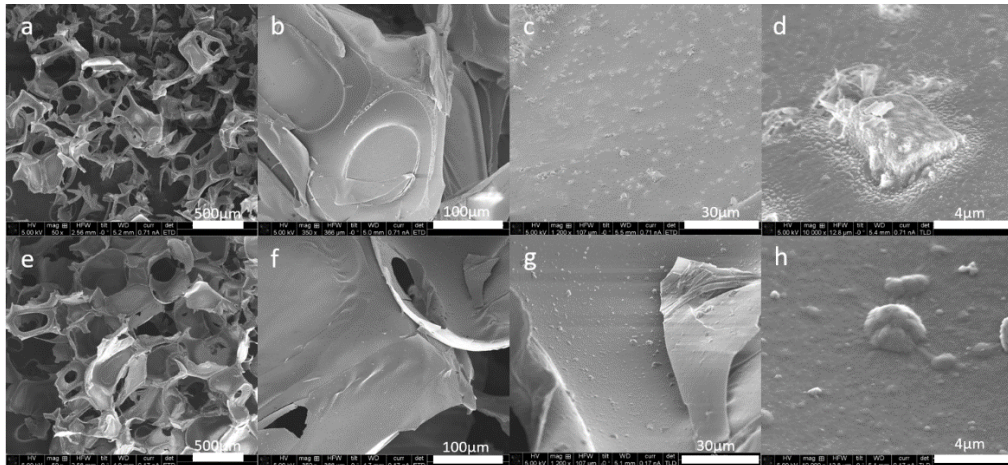


**Figure 1.11.** SEM image of residue char: a), b), c), d) residue of PUL50 and e), f), g), h) residue of PUL90.

## Flame retardancy discussion

The HRR profile of PUL90 sample was characterized by a sharp initial peak followed by quick drop down. A plateau was formed after then and gradually decreased to zero as combustion reach its end. Analysis of residue suggests that the strong charring is responsible for flammability improvement. Good char integrity was evidenced by the appearance (size and shape) of residue, implying that char presents nice mechanical property. Hence, barrier effect was preserved throughout the combustion as char did not prone have breakage when PUF shrinks during combustion. This overall pattern of flammability mitigation is comparable with that of LBL studies utilizing inorganic filler.<sup>12, 15, 33</sup> But the flammability of neat PUF in this study was lower than theirs. Otherwise, flame retardancy parameters in this study can have more drastic improvement. As it is illustrated in **Figure 1.12**, casein alone coated PUF did not have improvement and laponite coated PUF had a slight HRR reduction of secondary peak (both with approximately 5wt% coating uptake). This is further supporting evidence that the phosphorous component of casein has limited ability to impart anti-flammability with the very thin thickness level studied in the current work. When casein and laponite were combined in coating, a seemingly synergistic improvement could be found with PUL90. The thermal protection behavior of a similar very high filler content nanocomposite upon combustion has been discussed by Carosio and coworkers.<sup>34</sup> In their case, nanopapers with components of MMT clay in aggregated state and cellulose nanofiber(CNF) was made with clay concentration as high as 50%. This nanopaper was able to reduce PHRR from 285 KW/m<sup>2</sup> to 235 KW/m<sup>2</sup> and prolong TTI from 68 s to 299 s when hot pressed onto a glass fiber composite. The fire protection of polymer/ clay nanocomposite due to its isolating function was achieve in a smaller scenario

in this study. Stable char formation was favored by insufficient oxidation of casein resulted from high laponite filler concentration in addition to the cross-linking effect from phosphorous element. The protective char with volatile isolation was globally formed with enhancement by carbonaceous and clay filler combination.

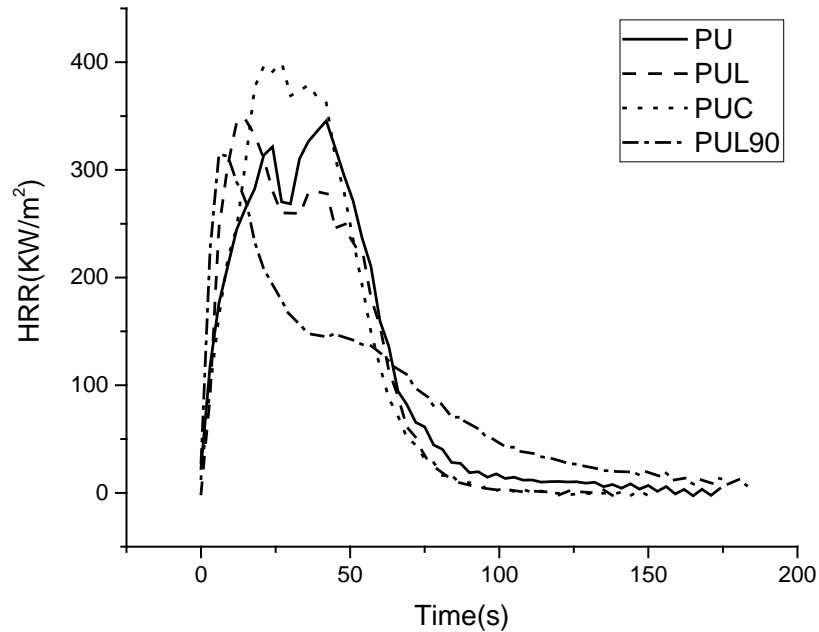


**Figure 1.12.** HRR profiles of PUFs coated with casein(PUC) or laponite(PUL), and PUL90, pure PU.

#### 1.4. Conclusion

In the current study, casein/ laponite nanocomposite coating was examined to demonstrate its ability in improving flammability of PUF. A one-pot dip coating fabrication method was utilized as simple and environmentally friendly method. Successful nanocomposite making with the nanofiller preferentially oriented along the x-y (plane) direction, although laponite was neither intercalated nor exfoliated, was confirmed with

FT-IR, XRD, and SEM in model system, with evidences that casein and laponite showed strong hydrogen bonding interaction and good dispersion of laponite nanoparticle. Casein/ laponite coating with 90wt% laponite concentration is able to reduce second HRR peak by 57.0% and aHRR by 30.9%. The other key factor-TSP of flammability was also reduced by 33.3% and melt dripping was eliminated. TGA analysis combined with SEM characterization of residue indicates that dominant flame retardant mechanism was barrier effect of promoted char forming by casein/ laponite coating. Above study indicates that casein/ laponite coating is potentially suitable candidate to endow flame retardancy to PUF with merits of green raw materials used, simple fabrication process, desirable flammability improvement, and abundant materials resource.

## 1.5. References

1. Haynes, H. J. G., Fire Loss in the United States during 2015. *National Fire Protection Association* **2016**.
2. Yang, R.; Hu, W.; Xu, L.; Song, Y.; Li, J., Synthesis, mechanical properties and fire behaviors of rigid polyurethane foam with a reactive flame retardant containing phosphazene and phosphate. *Polymer Degradation and Stability* **2015**, *122*, 102-109.
3. Robert C. Hale, M. L. G., Ellen Harvey, T. Matt Mainor, Potential role of fire retardant-treated polyurethane foam as a source of brominated diphenyl ethers to the US environment. *Chemosphere* **2002**, *46*, 729–735.
4. Chen, M.-J.; Chen, C.-R.; Tan, Y.; Huang, J.-Q.; Wang, X.-L.; Chen, L.; Wang, Y.-Z., Inherently Flame-Retardant Flexible Polyurethane Foam with Low Content of Phosphorus-Containing Cross-Linking Agent. *Industrial & Engineering Chemistry Research* **2014**, *53* (3), 1160-1171.
5. Wang, X.-L.; Yang, K.-K.; Wang, Y.-Z., Physical and chemical effects of diethylN,N'-diethanolaminomethylphosphate on flame retardancy of rigid polyurethane foam. *Journal of Applied Polymer Science* **2001**, *82* (2), 276-282.
6. Li, Y. C.; Schulz, J.; Grunlan, J. C., Polyelectrolyte/nanosilicate thin-film assemblies: influence of pH on growth, mechanical behavior, and flammability. *ACS Appl Mater Interfaces* **2009**, *1* (10), 2338-47.
7. Joshi, M.; Khanna, R.; Shekhar, R.; Jha, K., Chitosan nanocoating on cotton textile substrate using layer-by-layer self-assembly technique. *Journal of Applied Polymer Science* **2011**, *119* (5), 2793-2799.

8. Huang, G.; Liang, H.; Wang, X.; Gao, J., Poly(acrylic acid)/Clay Thin Films Assembled by Layer-by-Layer Deposition for Improving the Flame Retardancy Properties of Cotton. *Industrial & Engineering Chemistry Research* **2012**, 120914162412007.
9. Alongi, J.; Carosio, F.; Malucelli, G., Layer by layer complex architectures based on ammonium polyphosphate, chitosan and silica on polyester-cotton blends: flammability and combustion behaviour. *Cellulose* **2012**, 19 (3), 1041-1050.
10. Wang, Y.; Yang, X.; Peng, H.; Wang, F.; Liu, X.; Yang, Y.; Hao, J., Layer-by-Layer Assembly of Multifunctional Flame Retardant Based on Brucite, 3-Aminopropyltriethoxysilane, and Alginate and Its Applications in Ethylene-Vinyl Acetate Resin. *ACS Appl Mater Interfaces* **2016**, 8 (15), 9925-35.
11. Laufer, G.; Kirkland, C.; Cain, A. A.; Grunlan, J. C., Clay-chitosan nanobrick walls: completely renewable gas barrier and flame-retardant nanocoatings. *ACS Appl Mater Interfaces* **2012**, 4 (3), 1643-9.
12. Cain, A. A.; Plummer, M. G. B.; Murray, S. E.; Bolling, L.; Regev, O.; Grunlan, J. C., Iron-containing, high aspect ratio clay as nanoarmor that imparts substantial thermal/flame protection to polyurethane with a single electrostatically-deposited bilayer. *J. Mater. Chem. A* **2014**, 2 (41), 17609-17617.
13. Kim, Y. S.; Davis, R.; Cain, A. A.; Grunlan, J. C., Development of layer-by-layer assembled carbon nanofiber-filled coatings to reduce polyurethane foam flammability. *Polymer* **2011**, 52 (13), 2847-2855.
14. Kim, Y. S.; Harris, R.; Davis, R., Innovative Approach to Rapid Growth of Highly Clay-Filled Coatings on Porous Polyurethane Foam. *ACS Macro Letters* **2012**, 1 (7), 820-824.

15. Li, Y.-C.; Kim, Y. S.; Shields, J.; Davis, R., Controlling polyurethane foam flammability and mechanical behaviour by tailoring the composition of clay-based multilayer nanocoatings. *Journal of Materials Chemistry A* **2013**, *1* (41), 12987–12997.
16. Pan, Y.; Zhan, J.; Pan, H.; Wang, W.; Tang, G.; Song, L.; Hu, Y., Effect of Fully Biobased Coatings Constructed via Layer-by-Layer Assembly of Chitosan and Lignosulfonate on the Thermal, Flame Retardant, and Mechanical Properties of Flexible Polyurethane Foam. *ACS Sustainable Chemistry & Engineering* **2016**, *4* (3), 1431-1438.
17. Davis, R.; Li, Y. C.; Gervasio, M.; Luu, J.; Kim, Y. S., One-pot, bioinspired coatings to reduce the flammability of flexible polyurethane foams. *ACS Appl Mater Interfaces* **2015**, *7* (11), 6082-92.
18. Chen, H. B.; Shen, P.; Chen, M. J.; Zhao, H. B.; Schiraldi, D. A., Highly Efficient Flame Retardant Polyurethane Foam with Alginate/Clay Aerogel Coating. *ACS Appl Mater Interfaces* **2016**, *8* (47), 32557-32564.
19. Bellayer, S.; Jimenez, M.; Barrau, S.; Bourbigot, S., Fire retardant sol–gel coatings for flexible polyurethane foams. *RSC Adv.* **2016**, *6* (34), 28543-28554.
20. Gerard W. Hofland, M. v. E., Luuk A. M. van der Wielen, Geert-Jan Witkamp, Isoelectric Precipitation of Casein Using High-Pressure CO<sub>2</sub>. *Industrial & Engineering Chemistry Research* **1999**, *38*, 4919–4927.
21. Ghosh, A.; Ali, M. A.; Dias, G. J., Effect of cross-linking on microstructure and physical performance of casein protein. *Biomacromolecules* **2009**, *10* (7), 1681-8.
22. Siracusa, V.; Rocculi, P.; Romani, S.; Rosa, M. D., Biodegradable polymers for food packaging: a review. *Trends in Food Science & Technology* **2008**, *19* (12), 634-643.

23. Alongi, J.; Carletto, R. A.; Bosco, F.; Carosio, F.; Di Blasio, A.; Cuttica, F.; Antonucci, V.; Giordano, M.; Malucelli, G., Caseins and hydrophobins as novel green flame retardants for cotton fabrics. *Polymer Degradation and Stability* **2014**, *99*, 111-117.
24. Kiliaris, P.; Papaspyrides, C. D., Polymer/layered silicate (clay) nanocomposites: An overview of flame retardancy. *Progress in Polymer Science* **2010**, *35* (7), 902-958.
25. Ras, R. H.; Umemura, Y.; Johnston, C. T.; Yamagishi, A.; Schoonheydt, R. A., Ultrathin hybrid films of clay minerals. *Phys Chem Chem Phys* **2007**, *9* (8), 918-32.
26. P.L.M. Barreto, A. T. N. P., V. Soldi, Thermal degradation of edible films based on milk proteins and gelatin in inert atmosphere. *Polymer Degradation and Stability* **2003**, *79* (1), 147–152.
27. Pálková, H.; Madejová, J.; Zimowska, M.; Serwicka, E. M., Laponite-derived porous clay heterostructures: II. FTIR study of the structure evolution. *Microporous and Mesoporous Materials* **2010**, *127* (3), 237-244.
28. Nataliya S. Myshakina, Z. A., Sanford A. Asher, Dependence of Amide Vibrations on Hydrogen Bonding. *The Journal of Physical Chemistry B* **2008**.
29. Pierre Labbe; Reverdy, G., Adsorption characteristics of polycyclic aromatic compounds on clay pyrene as a photophysical probe on laponite. *Langmuir* **1988**, *4*, 419-425.
30. Zammarano, M.; Krämer, R. H.; Harris, R.; Ohlemiller, T. J.; Shields, J. R.; Rahatekar, S. S.; Lacerda, S.; Gilman, J. W., Flammability reduction of flexible polyurethane foams via carbon nanofiber network formation. *Polymers for Advanced Technologies* **2008**, *19* (6), 588-595.

31. Singh, H.; Jain, A. K., Ignition, combustion, toxicity, and fire retardancy of polyurethane foams: A comprehensive review. *Journal of Applied Polymer Science* **2008**, 1115-1143.
32. G. Camino, L. C., G. Martinasso, Intumescent fire-retardant systems. *Polymer Degradation and Stability* **1989**, 23 (4), 359-376.
33. Holder, K. M.; Cain, A. A.; Plummer, M. G.; Stevens, B. E.; Odenborg, P. K.; Morgan, A. B.; Grunlan, J. C., Carbon Nanotube Multilayer Nanocoatings Prevent Flame Spread on Flexible Polyurethane Foam. *Macromolecular Materials and Engineering* **2015**, n/a-n/a.
34. Carosio, F.; Kochumalayil, J.; Cuttica, F.; Camino, G.; Berglund, L., Oriented clay nanopaper from biobased components--mechanisms for superior fire protection properties. *ACS Appl Mater Interfaces* **2015**, 7 (10), 5847-56.

## Chapter 2.

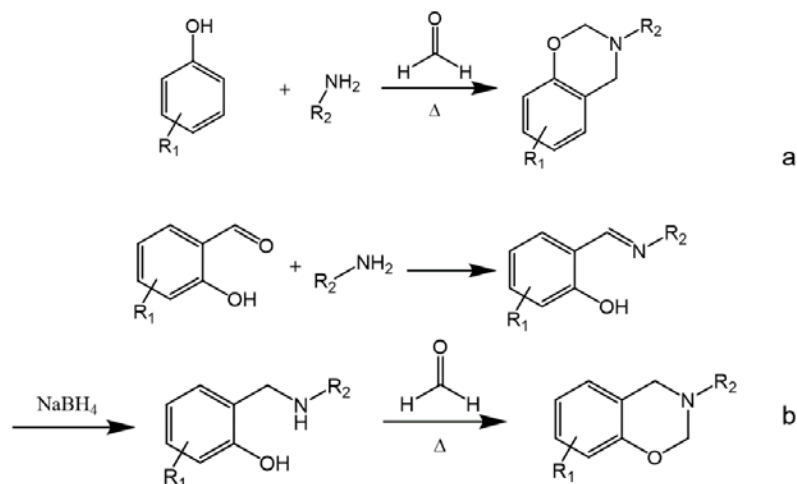
### Synthesis and Characterization of Fused-ring Benzo-/ naphthoxazines

#### Abstract

Fused-ring benzo/naphthoxazine monomers was synthesized from 1-naphthol, 1,5-dihydroxynaphthalene, or 3,5-dimethoxyphenol and cyclo-imines derived from piperidine, pyrrolidine. For the first time, their polymerization was confirmed by differential scanning calorimetry(DSC), thermogravimetric analysis(TGA), and fourier transform infrared spectroscopy(FT-IR). Similar thermal polymerization reaction with traditional benzoxazine monomers was found with oxazine ring disappearing and hydroxyl group forming by non-isothermal FT-IR experiment. Fused-ring monomers, studied in this work, presents significantly lowered polymerization temperature compared to benzoxazines without catalytic functional group. A particular bifunctional fused-ring naphthoxazine resin-poly(**15DHN-p-f**) showed attractive thermal stability-373°C 5% weight loss temperature and 43% char yield, which made this novel fused-ring monomer family of real world application potential.

## 2.1. Introduction

Polybenzoxazine is a new type of phenolic resin that has relatively recent been added to the list of commercially available thermoset materials.<sup>1</sup> The reasons are found in its outstanding physical and mechanical properties such as high char yield, resistance to flame, near-zero shrinkage, low water absorption, high glass transition temperature, and high modulus. The structure design flexibility of benzoxazine monomers is considered to be the highest among thermosets as it involves the reaction of widely commercially available phenols, primary amines and formaldehyde.<sup>2</sup> Less common methodologies have also been applied successfully for architectures where typical benzoxazine formation strategy was incompatible. The most used one of the alternative synthetic pathways is the 3-step strategy which involves the formation of a Mannich base through the reaction of a primary amine and a 2-hydroxybenzaldehyde and later reduction, usually with sodium borohydride, of the formed imine, and final closure of the ring with the use of formaldehyde (**Scheme 2.1**).<sup>3</sup> This strategy has been employed i.e. for the formation of hydroxyl functionalized benzoxazine,<sup>4</sup> aminostyrene based benzoxazines,<sup>5</sup> and cyanate ester containing benzoxazine.<sup>6</sup>



**Scheme 2.1.** Preparation of 1,3-benzoxazines through a) modified Mannich reaction of a phenol, primary amine and formaldehyde, and b) 3-step strategy.

Polymers possessing naphthalene group are expected to exhibit excellent mechanical property and thermal stability, resulting from high backbone rigidity and aromatic content provided by the polynuclear aromatic structure. Recent works have demonstrated the effectiveness of improving resin performance by incorporating naphthalene groups into backbone of various polymers, such as epoxy,<sup>7</sup> PAEK8, polyimide,<sup>9</sup> poly( $\epsilon$ -caprolactone),<sup>10</sup> and bismelamides.<sup>11</sup> Compared to the wide range of studies in benzoxazine chemistry, naphthoxazines have been paid lower attention to with few researches on synthesis and mechanical study on aniline based bifunctional naphthoxazines<sup>12</sup> and their degradation mechanism,<sup>13</sup> thin film from telechelic naphthoxazine polymer,<sup>14</sup> and thermal decomposition studies of aliphatic amine based naphthoxazines and its polymer.<sup>15</sup> Fused-ring naphthoxazines typically have a cycloaliphatic ring fused directly with oxazine ring. And they have been synthesized from 1-naphthol<sup>16</sup> or 2-naphthol<sup>17, 18</sup> as phenolic precursor with many alternative pathways for

organic chemistry studies. In this paper, a particular interest was carried out in 1-naphthol based fused-ring naphthoxazines because of the known superior resin performance of 1-polynaphthoxazines over 2-polynaphthoxazines.<sup>12</sup> For the first time to our knowledge, fused-ring naphthoxazines are investigated for their capability of polymerization and thermal stability of their resulting polymers.

## 2.2. Experimental Section

### 2.2.1. Materials

1-Naphthol (for synthesis) was purchase at EMD Millipore. 1,5-dihydroxynaphthalene (97%), 3,5-dimethoxyphenol (99%), N-Chlorosuccinimide (98%), piperidine (99%), pyrrolidine (99%), sodium methoxide (25wt% in methanol), sodium thiosulfate (99%), and 1,2,3,4-tetrahydroisoquinoline (95%) were used as received from Sigma-Aldrich. Acetonitrile (>99.9%), Alumina (neutral, 60-325 mesh), cyclohexane (>99.0%), dichloromethane (DCM) (>99.5%), diethyl ether (anhydrous, >99.0%), formaldehyde solution (37% wt. in water), hexanes(>98.5%), magnesium sulfate (anhydrous, certified grade)(MgSO<sub>4</sub>), sodium chloride(>99.0%), sodium hydroxide (NaOH) (>97%), and toluene (>99.5%) were obtained from Fisher Scientific and used as received. Synthesis of imines **1a-c** were prepared following reported method<sup>19</sup>.

### 2.2.2. Monomer synthesis

Synthesis of 8,9,10,10a-tetrahydro-6*H*-naphtho[2,1-*e*]pyrrolo[1,2-*c*][1,3]oxazine (Abbreviated as **1N-p-f**).

Betti reaction for the formation of aminocycloalkylnaphthol was conducted by following the procedure as described<sup>20</sup>. A solution of **1a** (0.284 g, 4.11 mmol, 1.2 eq.) in

DCM (3 mL) was added to a solution of 1-naphthol (0.494 g, 3.43 mmol) in DCM (3 mL). The reaction mixture was magnetically stirred in a sealed 15 mL vial at room temperature for 15 h. After evaporation of the solvent, diethyl ether (20 mL) was added and the organic phase was washed with a 0.5N NaOH aqueous solution (3 x 5 mL), brine (2 x 5 mL), and dried over MgSO<sub>4</sub>. The solvent was removed and the resulting product was dissolved in DCM (6 mL) and used without further purification, to which formaldehyde (37 wt.% in water, 0.83 mL, 10.3 mmol, 3 eq) was added in dropwise. The reaction mixture was stirred at room temperature overnight. After evaporation of the solvent, hexanes (30 mL) was added and the resulting suspension was filtered through a pad of alumina. Removal of the solvent afforded a transparent oil which crystallized on standing at low temperature (Yield: 55 %). <sup>1</sup>H-NMR (600 MHz, CDCl<sub>3</sub>, 20 °C) d, ppm: 8.15 (d, 1H, Ar), 7.74 (s, 1H, Ar), 7.47 (m, 2H, Ar), 7.10 (d, 1H, Ar), 5.12 (d, 1H, O-CH<sub>2</sub>-N), 5.07 (d, 1H, O-CH<sub>2</sub>-N), 4.76 (dd, 1H, Ar-CH-(CH<sub>2</sub>-)N), 3.23-1.78 (m, 6H, -N-CH<sub>2</sub>-CH<sub>2</sub>-CH<sub>2</sub>-CH(CH<sub>2</sub>-)). FT-IR n (cm<sup>-1</sup>): 2968-2876 (C-H alkane str.), 1325 (O-CH<sub>2</sub>-N wagg.), 1240 (C-O asym. str.), 1198 (C-N asym. str.), 1049 (C-O sym. Str.), and 924 (C-H out-of-plane naphthoxazine bend.).

Synthesis of 9,10,11,11a-tetrahydro-6*H*,8*H*-naphtho[2,1-*e*]pyrido[1,2-*c*][1,3]oxazine (Abbreviated as **1N-p6-f**).

A mixture of 1-Naphthol (0.99g, 6.87mmol) and **1b** (0.57g, 6.87mmol, 1 eq) in DCM (14mL) were stirred at room temperature for 24 h. the organic phase was washed with 0.5N NaOH aqueous solution (3 x 15mL) followed by water (2 x 15mL). After removal of solvent, resulting mixture was dissolved in 20mL and formaldehyde (37wt.% in water 0.61mL, 7.56mmol, 1.1 eq) was added. The reaction mixture was stirred at room temperature in 50mL round bottom flask for 12 h. Then solvent was evaporated and 50mL

hexanes was added to mixture. Resulting suspension was filtered through alumina pad. The final product was obtained as yellow solid (Yield: 74.2%). <sup>1</sup>H-NMR (600 MHz, CDCl<sub>3</sub>, 20 °C) d, ppm: 8.15 (dd, 1H, Ar) 7.75 (dd, 1H, Ar) 7.45 (m, 2H, Ar), 7.40 (d, 1H, Ar), 7.23 (d, 1H, Ar), 4.97(d, 1H, O-CH<sub>2</sub>-N), 4.86(d, 1H, O-CH<sub>2</sub>-N), 4.13(dd, 1H, Ar-CH(CH<sub>2</sub>-)-N), 3.02-1.56(m, 8H, -N-CH<sub>2</sub>-CH<sub>2</sub>-CH<sub>2</sub>-CH<sub>2</sub>-CH(CH<sub>2</sub>-)-). FT-IR n (cm<sup>-1</sup>): 2939-2748 (C-H alkane str.), 1333 (O-CH<sub>2</sub>-N wagg.) 1242 (O-C asym. str.), 1196 (C-N asym. str.), 1055 (C-O sym. str.), and 916 (C-H out-of-plane naphthoxazine bend.).

Synthesis of 9,13b-dihydro-6*H*,8*H*-naphtho[2',1':5,6] [1,3]oxazino[4,3-*a*]isoquinoline (Abbreviated as **1N-dhiq-f**).

A solution of **2c** (0.14 g, 1.07 mmol 1.2 eq) in DCM (2 mL) was added to a solution of 1-naphthol (1.29g, 0.89mmol). The reaction mixture was stirred for 24 h at room temperature in a sealed 15mL vial. After evaporation of the solvent, diethyl ether (10 mL) was added and the organic phase was washed with a 0.5N NaOH aqueous solution (3 x 5 mL), brine (2 x 5 mL), and dried over MgSO<sub>4</sub>. Then solvent was removed and resulting product was dissolved in DCM and used without further purification. To above mixture in a 15 mL vial, formaldehyde (37 wt.% in water, 0.26 mL, 3.21 mmol, 3 eq.) was added dropwise. Then the vial was sealed and the reaction mixture was magnetically stirred at room temperature overnight. After removal of the solvent, the crude product was washed with ethanol and acetone. Recrystallization in acetone afforded light orange-white crystals (Yield: 64%). <sup>1</sup>H-NMR (600 MHz, CDCl<sub>3</sub>, 20 °C) d, ppm: 8.20 (dd, 1H, Ar), 7.71 (dd, 1H, Ar), 7.48-7.42 (m, 3H, Ar), 7.33 (t, 1H, Ar), 7.28 (dt, 1H, Ar), 7.26 (d, 1H, Ar), 7.21 (d, 1H, Ar), 7.20 (d, 1H, Ar), 5.60 (d, 1H, Ar-CH(Ar)-N), 5.50 (d, 1H, O-CH<sub>2</sub>-N), 5.22 (d, 1H, O-CH<sub>2</sub>-N), 3.34-2.76 (m, 4H, N-CH<sub>2</sub>-CH<sub>2</sub>-Ar). FT-IR n (cm<sup>-1</sup>): 2988-2833 (C-H alkane

str.), 1331 (O-CH<sub>2</sub>-N wagg.), 1246 (C-O asym. str.), 1192 (C-N asym. str.), 1065 (C-O sym. Str.), and 920 (C-H oop naphthoxazine bend.).

Synthesis of 8,10-dimethoxy-1,2,3,10b-tetrahydro-5*H*-benzo[*e*]pyrrolo[1,2-*c*][1,3]oxazine (Abbreviated as **35DMP-p-f**).

A solution of **1a** (0.375 g, 5.43 mmol, 1.2 eq.) in DCM (4 mL) was added to a solution of 3,5-dimethoxyphenol (0.700 g, 4.53 mmol) in DCM (5 mL). The reaction mixture was magnetically stirred in a close 15 mL vial at room temperature overnight. After removal of the solvent, diethyl ether (50 mL) was added and the organic phase was washed with a 0.5N NaOH aqueous solution (3 x 10 mL), brine (2 x 10 mL), and dried over MgSO<sub>4</sub>. The solvent was removed and the resulting product was used without further purification. DCM (6 mL) was added to the crude product and formaldehyde (37 wt.% in water, 0.74 mL, 9.06 mmol, 2 eq) was added dropwise. The reaction mixture was stirred at room temperature overnight. After removal of the solvent, cyclohexane (20 mL) was added and the resulting suspension was filtered through a pad of alumina. Removal of the solvent afforded white crystals (Yield: 40 %). <sup>1</sup>H-NMR (600 MHz, CDCl<sub>3</sub>, 20 °C) d, ppm: 6.07 (d, 1H, Ar), 6.01 (s, 1H, Ar), 4.84 (dd, 1H, O-CH<sub>2</sub>-N), 4.78 (d, 1H, O-CH<sub>2</sub>-N), 4.52 (dd, 1H, Ar-CH(CH<sub>2</sub>-)-N), 3.76 (s, 3H, O-CH<sub>3</sub>), 3.75 (s, 3H, O-CH<sub>3</sub>), 3.16-1.73 (m, 6H, -N-CH<sub>2</sub>-CH<sub>2</sub>-CH<sub>2</sub>-CH(CH<sub>2</sub>-)-). FT-IR n (cm<sup>-1</sup>): 2964-2839 (C-H alkane str.), 1329 (O-CH<sub>2</sub>-N wagg.), 1238 (C-O asym. str.), 1200 (C-N asym. str.), 1053 (C-O sym. Str.), and 991 (C-H out-of-plane benzoxazine bend.).

Synthesis of 1,2,3,3a,9,10,11,11a-octahydro-7*H*,15*H*-dipyrrolo[1,2-*c*:1,2-*c'*]naphtho[2,1-*e*:6,5-*e'*]bis[1,3]oxazine (Abbreviation as **15DHN-p-f**).

To a solution 1,5-dihydroxynaphthalene (1.32 g, 8.21 mmol) in DCM (20 mL), a solution of 1a (1.25 g, 18.06 mmol, 2.2 eq.) in DCM (10 mL) was added. After 24 h being magnetically stirred at room temperature, the solvent was removed and the crude product was washed with hexane (2 x 20 mL). The resulting solid (2e) was dissolved in DCM (30 mL) and used without further purification. To the suspension, formaldehyde (37 wt.% in water, 1.67 mL, 20.53 mmol, 3 eq.) was added dropwise and the reaction mixture was magnetically stirred overnight at room temperature. After removal of the solvent, the crude product was dissolved in toluene (50 mL) and filtered through a pad of alumina, which was further washed with extra toluene (50 mL). After removal of the solvent, the resulting light brown crystals were washed with cold acetonitrile (Yield: 10%). <sup>1</sup>H-NMR (600 MHz, CDCl<sub>3</sub>, 20 °C) d, ppm: 7.70 (d, 1H, Ar), 7.10 (d, 1H, Ar), 5.10 (d, 1H, O-CH<sub>2</sub>-N), 5.03 (d, 1H, O-CH<sub>2</sub>-N), 4.73 (dd, 1H, Ar-CH-(CH<sub>2</sub>)-N), 3.23-1.73 (m, 6H, -N-CH<sub>2</sub>-CH<sub>2</sub>-CH<sub>2</sub>-CH(CH<sub>2</sub>-)). FT-IR n (cm<sup>-1</sup>): 2980-2860 (C-H alkane str.), 1321 (O-CH<sub>2</sub>-N wagg.), 1244 (C-O asym. str.), 1186 (C-N asym. str.), 1076 (C-O sym. Str.), and 966 (C-H oop naphthoxazine bend.).

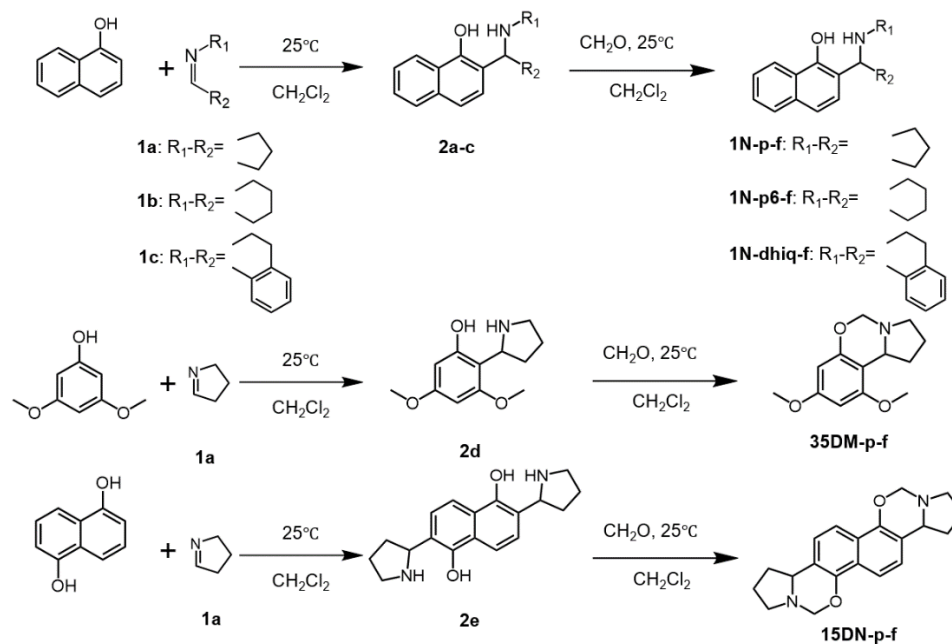
### 2.2.3. Characterization

<sup>1</sup>H nuclear magnetic resonance (NMR) spectra were acquired on a Varian Oxford AS600 at a proton frequency of 600 MHz. The average number of transients for <sup>1</sup>H measurement was 32, respectively. A relaxation time of 10 s was used for the integrated intensity determination of <sup>1</sup>H NMR spectra. Fourier transform infrared (FT-IR) spectra were recorded using a Bomem Michelson MB100 FT-IR spectrometer equipped with a

deuterated triglycine sulfate (DTGS) detector and a dry air purge unit. Co-addition of 64 scans were recorded at a resolution of  $4\text{ cm}^{-1}$ . A TA Instruments differential scanning calorimeter (DSC) Model 2920 was used with a heating rate of  $10\text{ }^{\circ}\text{C}/\text{min}$  and a nitrogen flow rate of  $60\text{ mL}/\text{min}$ . All samples were sealed in hermetic aluminum pans. Thermal decomposition of the reacted materials was determined by thermogravimetric analysis using a TA Instrument Model 2950 TGA. The TGA analysis was performed in a single heating run from room temperature to  $900\text{ }^{\circ}\text{C}$  at a heating rate of  $10\text{ }^{\circ}\text{C}/\text{min}$ , with a nitrogen flow rate of  $60\text{ mL}/\text{min}$ .

### **2.3. Results and Discussion**

Benzoxazine monomers are predominantly synthesized by performing variations of a generally modified Mannich reaction, and typically involves a phenol, a primary amine and formaldehyde. Although employed to a lesser extent, stepwise reaction involving the use 2-hydroxybenzaldehydes as a starting material has also been used especially in cases where the starting materials contained functional groups that were incompatible with the Mannich reaction. This methodology namely entails three steps: the formation of an imine by the reaction of a primary amine and the aldehyde, reduction to obtain a 2-aminoethylphenol, and closure of the ring by the use formaldehyde. In this study, another stepwise reaction is employed which gives rise to a novel type of polymerizable fused-ring benzoxazines or naphthoxazines. This approach involves the formation of first aminocycloalkylphenols by the Betti reaction of cyclic imines and activated phenols, followed by closure of the ring with formaldehyde.<sup>20</sup>



**Scheme 2.2.** Preparation of fused-ring benzo-/naphthoxazines.

The fused-ring benzo-/naphthoxazines synthesized in this study are prepared by using 1-naphthol, 3,5-dimethoxyphenol, and 1,5-dihydroxynaphthalene as activated phenols, and compounds **1a-c** as the cyclic imines (**Scheme 2.2**). The formation of aminocycloalkylphenols is carried out under mild conditions and affords the desired product with good yields. Closure of the ring is a straightforward reaction that is easily accomplished with formaldehyde at room temperature. All chemical structures were confirmed by <sup>1</sup>H-NMR. Unlike typical 1,3-oxazine proton singlets, the characteristic proton signals of the oxazine ring in the fused-ring benzo-/naphthoxazines ring, namely, the protons in position **a** and **b**, emerge as two doublets, respectively. The exception is found in compound **1N-dhiq-f** where the proton signal at position 4 emerges as a singlet due to the aromatic ring group of the dihydroquinoline. The rigid twisted-chair conformation of the fused-ring benzoxazines explains the differences between typical benzoxazine rings. **Figure 2.1** shows the <sup>1</sup>H-NMR spectra of the fused-ring benzo-

naphthoxazines and model benzoxazine PH-a. The complete  $^1\text{H-NMR}$  can be observed in the supporting information.

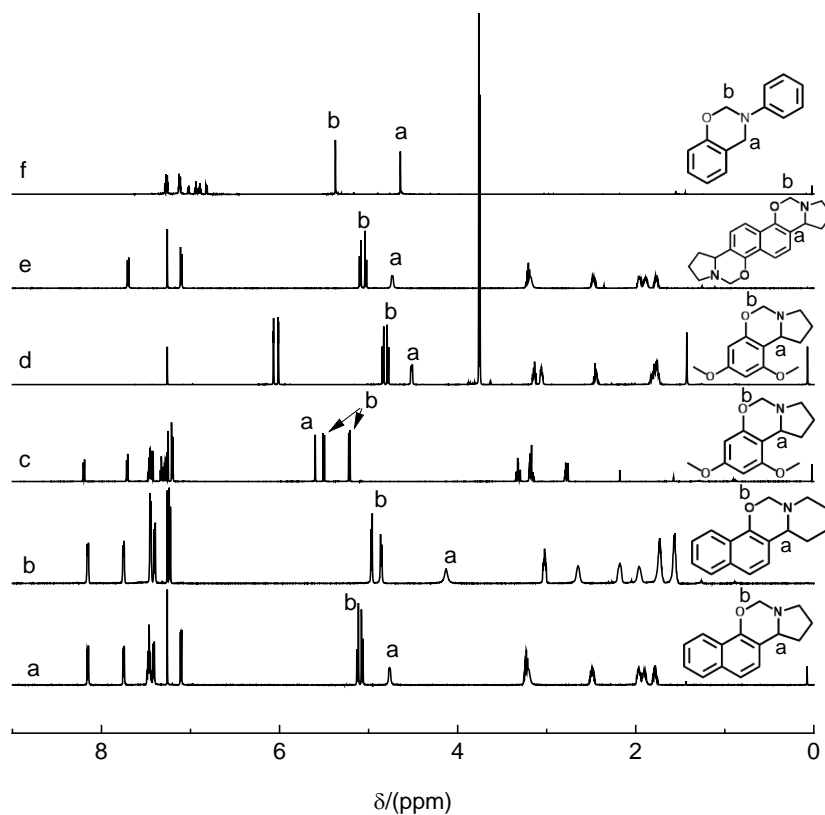


**Figure 2.1.**  $^1\text{H-NMR}$  spectra of a) **1N-p-f**, b) **1N-p6-f**, c) **1N-dihq-f**, d) **35DMP-p-f**, e) **15DHN-p-f**, and f) **PH-a**.

The structure of the fused-ring benzoxazines were also confirmed by FTIR analysis. **Figure 2.2** shows the FTIR spectra of **1N-p-f**, **1N-p6-f**, **1N-dhiq-f**, **35DMP-p-f**, and **15DHN-p-f** with characteristic bands of the oxazine ring modes highlighted. **Table 2.1** summarizes the characteristic values for  $\text{CH}_2$  wagging, C-O symmetric and asymmetric stretching, C-N asymmetric, and C-H out-of-plane vibration frequencies.

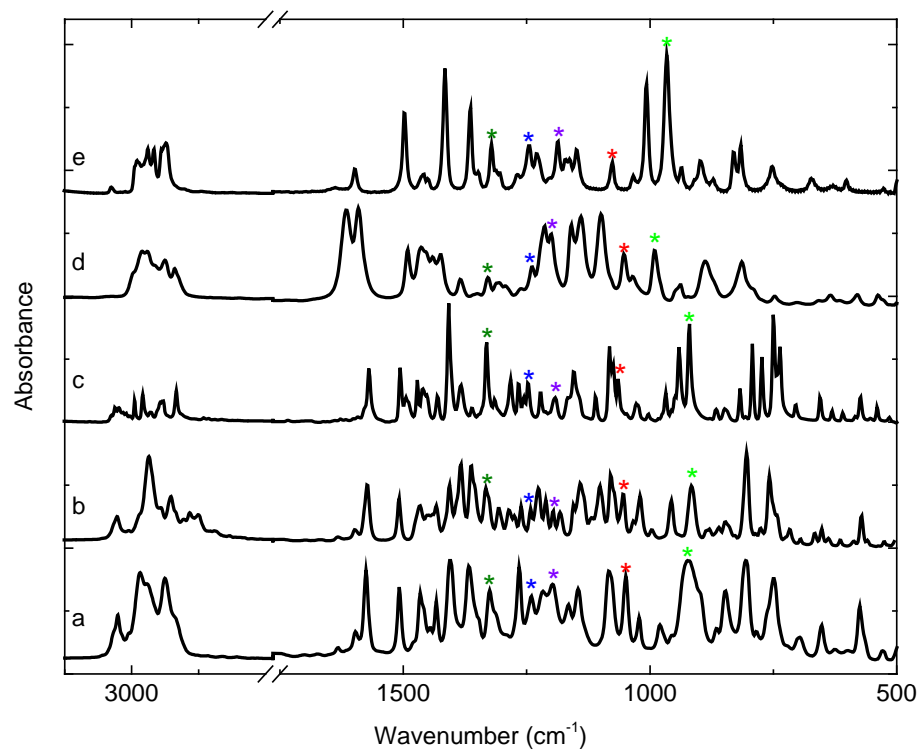


**Figure 2.2.** FT-IR spectra of a) **1N-p-f**, b) **1N-p6-f**, c) **1N-dihq-f**, d) **35DMP-p-f**, and e) **15DHN-p-f**. Colored asterisks indicate characteristic modes for oxazine ring: -CH<sub>2</sub> wagging (\*), C-O asymmetric str. (\*), C-N asymmetric str. (\*), C-O symmetric str. (\*), and C-H out-of-plane bend. (\*).

**Table 2.1.** Characteristic vibration frequencies for oxazine ring for fused-ring benzo-  
/naphthoxazines.

Compound	Vibration frequency (cm <sup>-1</sup> )				
	CH <sub>2</sub> wagg.	C-O asym.	C-N asym.	C-O sym.	Oop Benz/Naphth.*
<b>1N-p-f</b>	1325	1240	1198	1049	924
<b>1N-p6-f</b>	1333	1242	1196	1055	916
<b>1N-dhiq-f</b>	1331	1246	1192	1065	920
<b>35DMP-p-f</b>	1329	1238	1200	1053	991 (937 w)
<b>15DHN-p-f</b>	1321	1244	1186	1076	966

\* Oop = out-of-plane.

In addition, **Figure 2.3** shows the FT-IR spectra of fused-ring naphthoxazines in the region 1000-500 cm<sup>-1</sup> region. The bands in the region 900-650 cm<sup>-1</sup> are associated with out-of-plane C-H bending vibrations of substituted naphthalenes whose positions have been correlated with the number of adjacent hydrogen atoms in the aromatic rings. A common feature in all the fused-ring naphthoxazines synthesized in this study is the presence of two adjacent hydrogen atoms (position **3** and **4**) whose C-H out-of-plane bending vibration can be clearly observed between 816-793 cm<sup>-1</sup>. Additionally, **1N-p-f**, **1N-p6-f**, and **1N-dhiq-f** show strong pair of bands between 762-735 cm<sup>-1</sup> which are associated with C-H out-of-plane bending of four adjacent hydrogen atoms (position **5**, **6**, **7**, and **8**). Although **15DHN-p-f** also possesses a band in this region, it is not considered to be of the same nature as its characteristics differ importantly with those of the other fused-ring naphthoxazines. Furthermore, the characteristic band due to out-of-plane ring deformation vibration in

disubstituted naphthalenes can be observed centered at  $653\text{ cm}^{-1}$  for **1N-p-f**, **1N-p6-f**, and **1N-dhiq-f**. The highlighted extra bands emerging from the FT-IR spectrum of **1N-dhiq-f** are associated to the C-H out-of-plane bending vibration of the four adjacent hydrogen atoms in the dihydroisoquinoline moiety of the compound.

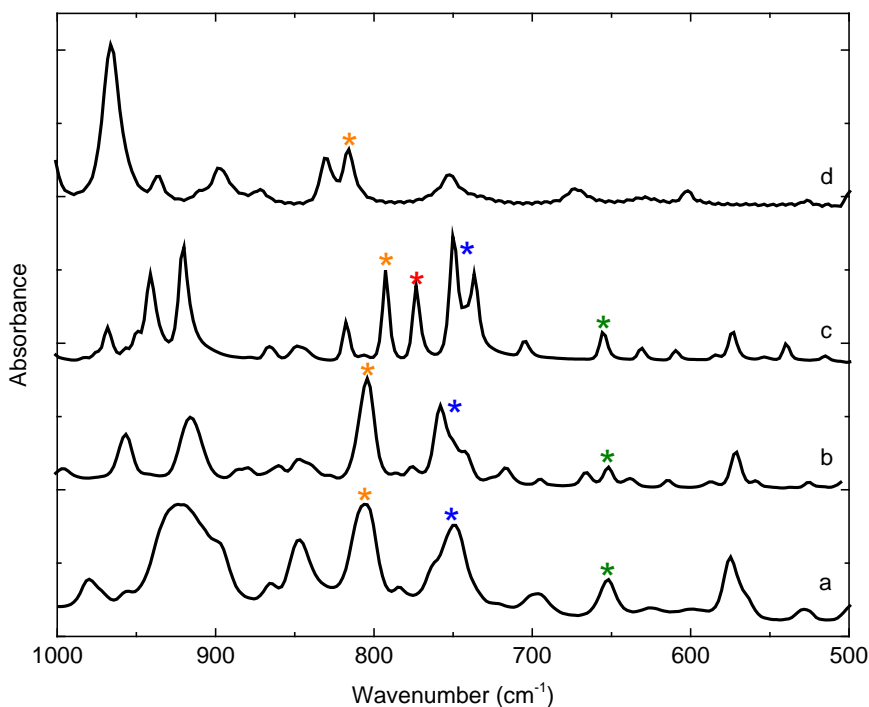


**Figure 2.3.** FT-IR spectra of a) **1N-p-f**, b) **1N-p6-f**, c) **1N-dihq-f**, and e) **15DHN-p-f**.

### **Thermal behavior of fused-ring benzo-/naphthoxazines**

The thermal behavior of the fused-ring benzo/naphthoxazines was studied by differential scanning calorimetry. The thermograms of all the compounds are shown in **Figure 2.4** along with model benzoxazine PH-a.

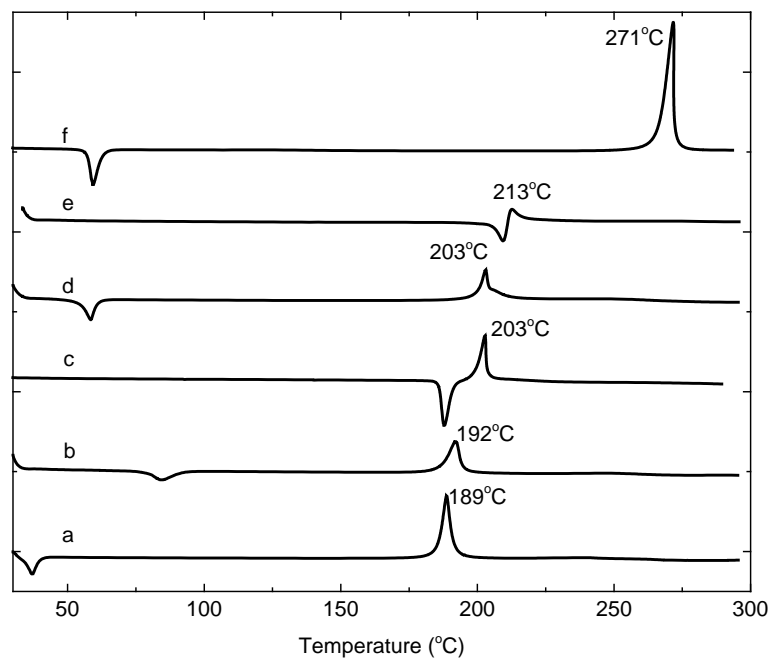


**Figure 2.4.** DSC thermograms of a) **1N-p-f**, b) **1N-p6-f**, c) **1N-dihq-f**, d) **35DMP-p-f**, e) **15DHN-p-f**, and f) PH-a.

All the thermograms show both an endothermic and exothermic event which are attributed to melting and ring-opening reaction of the different compounds, respectively. It is worth noting the considerably lower temperature for the ring-opening reaction of all the fused-ring benzo-/naphthoxazines when compared to that of model PH-a. Thus, the ring-opening reaction temperature for **1N-p-f**, **1N-p6-f**, **1N-dihq-f**, and **35DMP-p-f** are 189, 192, 203, and 203 °C, respectively. Bifunctional **15DHN-p-f** possesses an exothermic maximum peak at relatively higher temperature of 213 °C. However, the reaction for this compound occurs at the same time the melting takes place. It sounds then reasonable to expect a ring-opening reaction of **15DHN-p-f** at similar temperatures as the other benzo-/naphthoxazines, were not for the movement restriction of the molecules in the crystalline

state. It should be stressed, nonetheless, the low ring-opening reaction temperature of these fused-ring benzo-/naphthoxazines as there is no catalytic functionality in their chemical structures. Benzoxazines containing carboxylic moieties,<sup>21</sup> and benzoxazines containing hydrogen bond forming functional groups have shown lower than ordinary polymerization temperature.<sup>22</sup> However, it is rather unusual to observe such low ring-opening reaction temperature at these low temperatures without those aforementioned driving forces. A reason for the reduction of the reaction temperature might be found in ring strain instabilities of the fused-ring benzo-/naphthoxazines. Thus, the lowest exothermic temperature recorded in this study is for **1N-p-f** which contains a five-membered ring fused to the oxazine ring in its structure.

### **Ring-opening reaction of fused-ring benzo-/naphthoxazines**

FT-IR analysis was also used to study the ring-opening reaction of **1N-p-f**. **Figure 2.5** shows the FTIR spectra of a sample of **1N-p-f** at room temperature and heated at 120 °C for 1h, 130 °C for 30 min, 140 °C for 30 min, and 150 °C for 30 min.

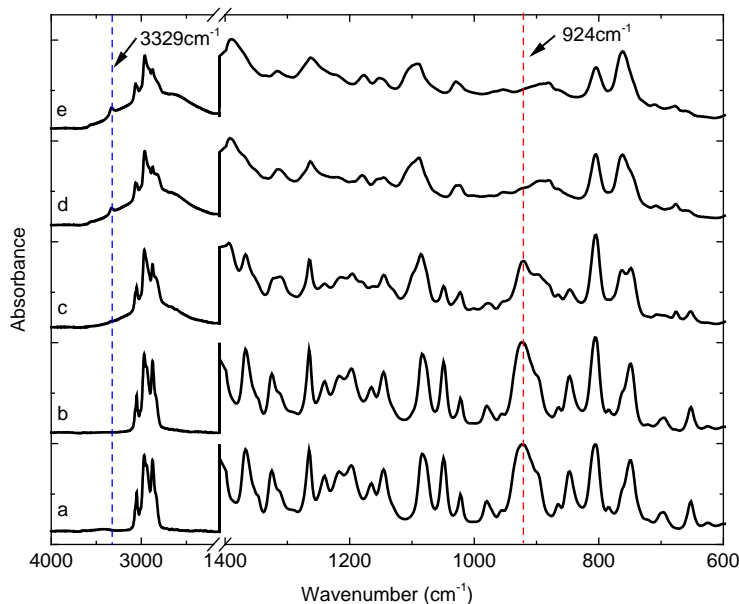


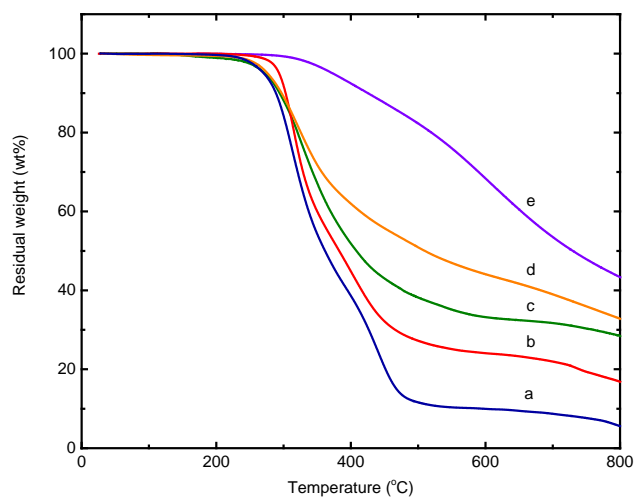
**Figure 2.5.** FT-IR spectra of **1N-p-f** between the regions 4000-600  $\text{cm}^{-1}$  at a) rt, b) 120  $^{\circ}\text{C}$  for 1h, c) 130  $^{\circ}\text{C}$  for 30 min, d) 140  $^{\circ}\text{C}$  for 30 min, and e) 150  $^{\circ}\text{C}$  for 30 min.

Characteristic bands associated to oxazine ring clearly vanished as **1N-p-f** was subjected to increasing temperatures, namely, 1325, 1240, 1198, 1049, and 924  $\text{cm}^{-1}$  (see **Table 2.1** for their assignation). Consequently, the O-H stretching vibration band of the open-ring structure could clearly be observed emerging at 3329  $\text{cm}^{-1}$ . Interestingly, the region in the FT-IR spectra between 900 and 600  $\text{cm}^{-1}$ , associated with out-of-plane C-H bending vibrations of substituted naphthalenes, was also affected with increasing temperature. As the band due the two adjacent hydrogen atoms (oop C-H bend.) at 806  $\text{cm}^{-1}$  decreased, the pair of bands centered at 755  $\text{cm}^{-1}$ , associated to the four adjacent hydrogen atoms (oop C-H bend.), experienced a clear change in shape. At the same time, a new band of medium-weak nature appeared at 881  $\text{cm}^{-1}$ . This band lies in the region associated to out-of-plane C-H bending of an isolated hydrogen atom in a substituted naphthalene,

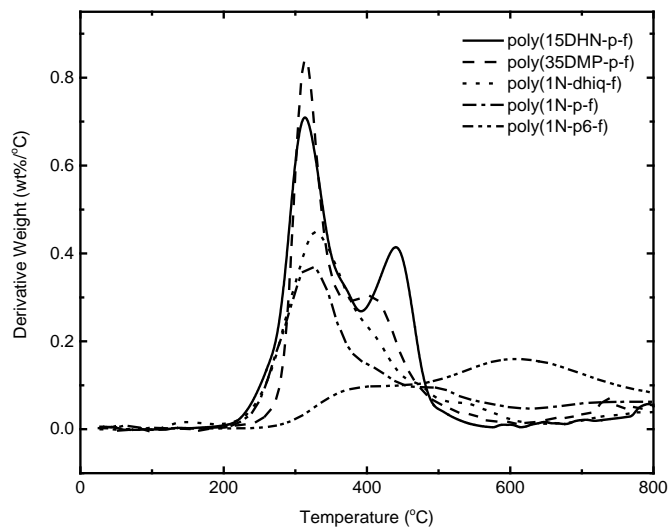
namely, between 900 and 855  $\text{cm}^{-1}$ . Furthermore, characteristic band due to out-of-plane ring deformation vibration in disubstituted naphthalenes at 653  $\text{cm}^{-1}$ , common in all the fused-ring benzoxazines, decreased as temperature increased. What this seems to suggest is that, according to the proposed mechanism of ring-opening reaction of benzoxazine, after the ring-opening step, the subsequent electrophilic substitution occurs at the free para position (position **4**) of the naphthol. However, substitutions in other position than **4** in the naphthol should not be discarded. Thus, substitution in the position either **6** or **7** would also generate bands associated to out-of-plane C-H bending of both an isolated hydrogen and two adjacent hydrogen atoms. Substitution in position either **5** or **8** would, however, generate new bands in the region 820-730  $\text{cm}^{-1}$  due to out-of-plane C-H bending of three adjacent hydrogen atoms, which could not be observed.

### **Thermal Stability**

The fused-ring benzo-/naphthoxazines were subjected to heat treatment 150, 180, 200, and 220 °C for 1 h each, with the exception of **15DHN-p-f** which was heated further at 250 °C for 30 min. The resulting materials were studied by thermogravimetric analysis (TGA). The results are shown in **Figure 2.6**.



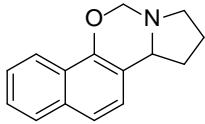
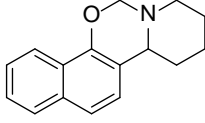
**Figure 2.6.** TGA thermograms of a) **poly(1N-p6-f)**, b) **poly(1N-p-f)**, c) **poly(1N-dhiq-f)**, d) **poly(35DMP-p-f)**, and e) **poly(15DHN-p-f)**.

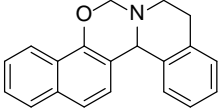
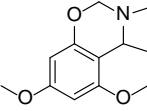
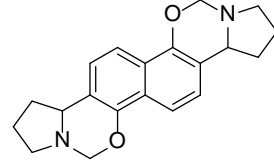


**Figure 2.7.** Derivative of the weight loss as a function of the temperature of the fused-ring benzo-/naphthoxazines.

As it can be observed from the **Figure 2.6**, all the polymers of fused-ring benzo-/naphthoxazines prepared in this study showed a certainly similar degradation profile. Two main degradation steps are observed from the first derivative curves (**Figure 2.6**), being the first one where most of the weight loss occurs. There seems to exist an expected pattern in the thermal stability dependency on the aliphatic content of the fused-ring benzo-/naphthoxazines. Thus, the monomer with the highest aliphatic content, the six-member fused-ring naphthoxazine **1N-p6-f**, generates a polymer that produces the lowest char yield of 6%. An outcome that is systematically improved as the aliphatic content diminishes as in poly(**1N-p-f**) (17%) and even further as in poly(**1N-dhiq-f**) (26%). Expectedly, bifunctional **15DHN-p-f** produces a thermoset with a much enhanced thermal stability due most likely to higher degree of crosslinking. The greater thermal stability of poly(**1N-p-f**) is not only observed in the resulting char yield (43%) but also in both  $T_{d5}$  and  $T_{d10}$  values of 373 and 425 °C, respectively. **Table 2.2** summarizes the thermal stability values of the polymers.

**Table 2.2.** Thermal stability values of polymerized fused-ring benzo-/naphthoxazines.

Monomer	Polymer Abbr.	$T_{d5}$ (°C)	$T_{d10}$ (°C)	Char yield
	poly( <b>1N-p-f</b> )	293	303	17
	poly( <b>1N-p6-f</b> )	271	369	6

	poly( <b>1N-dhiq-f</b> )	272	294	28
	poly( <b>35DMP-p-f</b> )	276	297	33
	poly( <b>15DHN-p-f</b> )	373	425	43

## 2.4. Conclusions

A new class of benzo or naphthoxazines, namely fused-ring benzo/naphthoxazines, are reported for the first time for their nature of forming polymers. Strong evidence supporting polymerization behavior of these novel monomers was found with FT-IR in cumulative heating experiment, indicating a similar ring-opening reaction upon thermal polymerization. Together with thermal behavior investigation by DSC studies, significantly lower polymerization temperature than traditional benzoxazine monomers without catalytical moiety was confirmed which can be attributed to higher strain carried by fused-ring monomers. Additionally, thermal stability results from TGA give raise to a specific polymer-poly(**15DHN-p-f**) possessing high  $T_{d5}$ (373 °C) and char yield (43%), whose property is comparable to traditional polybenzoxazine resins.

## 2.5. References

1. H. I. a. D. j. ALLEN, *Journal of Polymer Science Part B: Polymer Physics*, 1996, **34**, 1019-1030.
2. Y. Yagci, B. Kiskan and N. N. Ghosh, *Journal of Polymer Science Part A: Polymer Chemistry*, 2009, **47**, 5565-5576.
3. R. Andreu and J. C. Ronda, *Synthetic Communications*, 2008, **38**, 2316-2329.
4. C. H. Lin, H. T. Lin, S. L. Chang, H. J. Hwang, Y. M. Hu, Y. R. Taso and W. C. Su, *Polymer*, 2009, **50**, 2264-2272.
5. Y.-X. Liu, H.-M. Ma, Y. Liu, J.-J. Qiu and C.-M. Liu, *Polymer*, 2016, **82**, 32-39.
6. S. Ohashi, J. Kilbane, T. Heyl and H. Ishida, *Macromolecules*, 2015, **48**, 8412-8417.
7. T. E. MASASHI KAJI, *Journal of Polymer Science Part A: Polymer Chemistry*, 1999, **37**, 3063-3069.
8. T. T. a. Mami Ohno and T. Endo, *Macromolecules*, 1994, **23**, 3447-3448.
9. F.-C. C. Der-Jang Liaw, M.-Y. C. Man-kit Leung, and and K. Muellen, *Macromolecules*, 2004, **38**, 4024-4029.
10. B. Kiskan and Y. Yagci, *Polymer*, 2005, **46**, 11690-11697.
11. C.-S. W. a. H.-J. HWANC, *Journal of Polymer Science Part A: Polymer Chemistry*, 1996, **34**, 1493-1500.
12. S. B. S. a. H. ISHIDA, *journal of Applied Polymer Science*, 1996, **61**, 1595-1605.
13. T. Uyar, Z. Koyuncu, H. Ishida and J. Hecaloglu, *Polymer Degradation and Stability*, 2008, **93**, 2096-2103.
14. A. Yildirim, B. Kiskan, A. L. Demirel and Y. Yagci, *European Polymer Journal*, 2006, **42**, 3006-3014.

15. T. Uyar, J. Hacaloglu and H. Ishida, *Journal of Applied Polymer Science*, 2013, **127**, 3114-3123.
16. M. Heydenreich, A. Koch, I. Szatmári, F. Fülöp and E. Kleinpeter, *Tetrahedron*, 2008, **64**, 7378-7385.
17. M. L. Deb, S. S. Dey, I. Bento, M. T. Barros and C. D. Maycock, *Angew Chem Int Ed Engl*, 2013, **52**, 9791-9795.
18. S. Mahato, S. Haldar and C. K. Jana, *Chem Commun (Camb)*, 2014, **50**, 332-334.
19. E. Gravel, E. Poupon and R. Hocquemiller, *Tetrahedron*, 2006, **62**, 5248-5253.
20. C. Cimorelli, D. Fratoni, A. Mazzanti and G. Palmieri, *European Journal of Organic Chemistry*, 2011, **2011**, 2094-2100.
21. R. Andreu, J. A. Reina and J. C. Ronda, *Journal of Polymer Science Part A: Polymer Chemistry*, 2008, **46**, 6091-6101.
22. K. Zhang and H. Ishida, *Polym. Chem.*, 2015, **6**, 2541-2550.